AFAPL-TR-71-39

DEVELOPMENT OF A PLANAR HEAT PIPE FOR COOLING LARGE CAPACITY BATTERIES

E. T. MAHEFKEY, JR.

DECEMBER 1971

AIR FORCE AERO PROPULSION LABORATORY
AIR FORCE SYSTEMS COMMAND
WRIGHT-PATTERSON AIR FORCE BASE, OHIO

NOTICE

When Government drawings, specifications, or other data are used for any purpose other than in connection with a definitely related Government procurement operation, the United States Government thereby incurs no responsibility nor any obligation whatsoever; and the fact that the government may have formulated, furnished, or in any way supplied the said drawings, specifications, or other data, is not to be regarded by implication or otherwise as in any manner licensing the holder or any other person or corporation, or conveying any rights or permission to manufacture, use, or sell any patented invention that may in any way be related thereto.

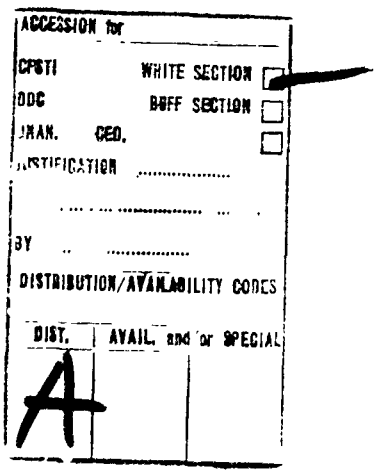

Copies of this report should not be returned unless return is required by security considerations, contractual obligations, or notice on a specific document.

AIR FORCE 25-2-72/100

UNCLASSIFIED
Security Classification

DOCUMENT CONTROL DATA - R & D

(Security classification of title, body of abstract and indexing annotation must be entered when the overall report is classified)

1 ORIGINATING ACTIVITY (Corporate author)	2a. REPORT SECURITY CLASSIFICATION
Air Force Systems Command AF Aero Propulsion Laboratory Wright-Patterson Air Force Base, Ohio	Unclassified 2b. GROUP

3 REPORT TITLE

DEVELOPMENT OF A PLANAR HEAT PIPE FOR COOLING LARGE CAPACITY PATTERIES

4 DESCRIPTIVE NOTES (Type of report and inclusive dates)

5 AUTHOR(S) (First name, middle initial, last name)

E. T. Mahefkey, Jr.

6 REPORT DATE	7a. TOTAL NO OF PAGES	7b. NO OF REFS
December 1971	96	29

8a. CONTRACT OR GRANT NO	9a. ORIGINATOR'S REPORT NUMBER(S)
b. PROJECT NO 3145	AFAPL-TR-71-39
c.	9b. OTHER REPORT NO(S) (Any other numbers that may be assigned this report)
d.	

10 DISTRIBUTION STATEMENT

This document has been approved for public release and sale; its distribution is unlimited.

11 SUPPLEMENTARY NOTES	12 SPONSORING MILITARY ACTIVITY
	Air Force Aero Propulsion Laboratory Wright-Patterson Air Force Base, Ohio

13 ABSTRACT

A planar (rectangular cross section) heat pipe was fabricated and tested using electrical heaters to simulate battery waste heat. The device was constructed of 0.025" stainless steel, with two layers of 100-mesh stainless steel screen as a capillary wick; water was used as the working fluid. Transient and steady state response was investigated. External axial temperature profiles were measured for 5, 12, and 20 watts applied power; internal evaporator and condenser temperatures were also measured.

Operation of the device was stable and repeatable within a temperature range of 50 to 180°F; no temperature or pressure fluctuations were noted. Mean external axial thermal resistance of 0.194 and 0.067°F/BTU/hr were calculated from experimental results for 5 and 20 watts (17.06 and 68.24 BTU/hr) input power, respectively. Evaporator film heat transfer coefficients of 18.6 and 53.3 BTU/hr ft^2 F were calculated based on observed temperature gradients for input power densities of 61.4 BTU/hr ft^2 at 5 watts and 245.6 BTU/hr ft^2 at 20 watts, respectively.

A comparison of the external axial temperature profile for the heat pipe with that of solid metal fins showed the heat pipe offers a significant advantage in temperature control and/or weight. The temperature profile for the heat pipe and the solid copper fin compared closely for most tests but the heat pipe had a distinct advantage over the aluminum fin. Maximum heat source temperature with the heat pipe was 118°F for 20 watts applied power, as compared to 146 F for the aluminum fin.

DD FORM 1 NOV 68 1473

UNCLASSIFIED
Security Classification

14 KEY WORDS	LINK A		LINK B		LINK C	
	ROLE	WT	ROLE	WT	ROLE	WT
Heat Pipe Heat Transfer Secondary Batteries Thermal Effects, Battery Performance						

U S Government Printing Office 1972 759-082/365

AFAPL-TR-71-39

DEVELOPMENT OF A PLANAR HEAT PIPE FOR COOLING LARGE CAPACITY BATTERIES

E. T. MAHEFKEY, JR.

FOREWORD

The work described in this report was conducted in the Aerospace Power Division of the Air Force Aero Propulsion Laboratory under Project 3145, Task 314522WE. The effort extended from January 1970 to September 1970, and formed the basis of a thesis for the degree of Master of Science from the University of Dayton, Department of Physics. This report was submitted by the author in November 1970.

The assistance provided by Mr. Stanley Douple, Air Force Aero Propulsion Laboratory, in assembling the experimental apparatus is sincerely appreciated. The advise and assistance of Dr. John Lander, Air Force Aero Propulsion Laboratory, and Professor Marshall Kreitman, Department of Physics, University of Dayton, are sincerely appreciated.

Donald P. Mortel

DONALD P. MORTEL
Acting Chief, Energy Conversion Branch
Aerospace Power Division
Air Force Aero Propulsion Laboratory

ABSTRACT

A planar (rectangular cross section) heat pipe was fabricated and tested using electrical heaters to simulate battery waste heat. The device was constructed of 0.025" stainless steel, with two layers of 100-mesh stainless steel screen as a capillary wick; water was used as the working fluid. Transient and steady state response was investigated. External axial temperature profiles were measured for 5, 12, and 20 watts applied power; internal evaporator and condenser temperatures were also measured.

Operation of the device was stable and repeatable within a temperature range of 50 to 180°F; no temperature or pressure fluctuations were noted. Mean external axial thermal resistance of 0.194 and 0.067°F/BTU/hour were calculated from experimental results for 5 and 20 watts (17.06 and 68.24 BTU/hr) input power, respectively. Evaporator film heat transfer coefficients of 18.6 and 53.3 BTU/hr ft^2°F were calculated based on observed temperature gradients for input power densities of 61.4 BTU/hr ft^2 at 5 watts and 245.6 BTU/hr ft^2 at 20 watts, respectively.

Comparison of the external axial temperature profile for the heat pipe with that of solid metal fins showed the heat pipe offers a significant advantage in temperature control and/or weight. The temperature profile for the heat pipe and the solid copper fin compared closely for most tests, but the heat pipe had a distinct advantage over the aluminum fin. Maximum heat source temperature with the heat pipe was 118°F for 20 watts applied power, as compared to 146°F for the aluminum fin.

TABLE OF CONTENTS

SECTION		PAGE
I	INTRODUCTION	1
II	THEORY OF PERFORMANCE	3
	1. The Heat Pipe	3
	2. Fundamental Capillary Physics	3
	a. The Law of Laplace and Young	3
	b. The Capillary Pump	4
	c. Fluid Flow in Porous Media/Darcy's Law	7
	3. Vapor Flow in a Rectangular Channel	10
	4. Vapor Generation and Condensation in Capillary Wick	10
	5. Analytical Model of Planar Heat Pipe	12
III	DESCRIPTION OF EXPERIMENTS AND APPARATUS	13
	1. Approach	13
	2. Planar Heat Pipe Configuration, Materials, and Fabrication	13
	3. Cleaning and Loading Procedures	16
	4. Working Fluid Preparation	21
	5. Instrumentation and Electrical Testing Apparatus	21
	6. Test Description	26
	a. Forced Convection Cooled Tests	26
	b. Radiation Cooled Tests	26
	c. Copper and Aluminum Fin Tests	28
IV	EXPERIMENTAL RESULTS	32
	1. General	32
	2. Forced Convection Cooled Test Results	32
	a. Demonstrated Heat Pipe Mode of Operation	32

TABLE OF CONTENTS (Contd)

SECTION			PAGE
		b. Temperature Profile as a Function of Applied Power	32
		c. Influence of Gravity on Temperature Profile	35
		d. Variation in Amount of Working Fluid	35
	3.	Radiation Cooled Tests	39
	4.	Comparative Temperature Profiles for Solid Copper and Aluminum Fins	42
V		ANALYSIS OF TEST RESULTS	51
	1.	Estimate of Experimental Error	51
		a. Thermocouple Measurements	51
		b. Pressure Measurements	51
		c. Power Measurements	51
		d. Evaporator Insulation Losses	51
		e. Overall Experimental Error	52
	2.	Correlation of Internal Temperature Measurements	53
	3.	Mean Axial and Radial Temperature Gradients	58
		a. Thermal Resistance of Heat Pipe	58
		b. Film Heat Transfer Coefficient Calculation	61
	4.	Analysis of Capillary Properties of Stainless Steel Screen Wick	63
	5.	Heat Pipe Design Refinement	66
VI		CONCLUSIONS AND RECOMMENDATIONS	67
APPENDIXES			
I		Calculation of Vapor Injection Velocity and Axial Pressure Loss in Rectangular Channel	69
II		Calculation of Temperature Gradient in Capillary Wick	71

TABLE OF CONTENTS (Contd)

SECTION		PAGE
III	Calculated Maximum Heat Transfer Rate of Planar Heat Pipe	73
IV	Calculations of the Amount of Water Necessary to Saturate Capillary Wick	75
V	Vaporization Rate Calculations for Nonequilibrium Operation	76
REFERENCES		77

LIST OF FIGURES

FIGURE		PAGE
1.	Two-Dimensional Model of Planar Heat Pipe	5
2.	Darcy's Experiment	8
3.	Several Experimental Heat Pipes	14
4.	Assembled Planar Heat Pipe	17
5.	Assembly Drawing of Planar Heat Pipe	18
6.	Filling Apparatus for Planar Heat Pipe	19
7.	Schematic Diagram of Filling System	20
8.	Copper Heat Source	22
9.	Pressure Transducer Calibration Curve	25
10.	Planar Heat Pipe on Laboratory Clean Bench Station	27
11.	Vacuum Chamber Test Setup and Measurement Apparatus	29
12.	Copper and Aluminum Fins Shown with Planar Heat Pipe	30
13.	Copper Fin Installed in Vacuum Chamber Cryowall	31
14.	Results of Planar Heat Pipe Operation in Three Modes	33
15.	Planar Heat Pipe Axial Temperature Profile as a Function of Applied Power, Near Horizontal, Forced Convection Tests	34
16.	The Influence of Gravity on Planar Heat Pipe Axial Temperature Profile	36
17.	Effect of the Amount of Working Fluid on Planar Heat Pipe Performance, — Forced Convection One Hour Test, Near Horizontal Position	38
18.	Transient Thermal Response for Planar Heat Pipe, -320°F Radiation Heat Sink Test	40
19.	Transient Thermal Response for Planar Heat Pipe, -50°F Radiation Heat Sink Test	41
20.	Equilibrium Axial Temperature Profile for Planar Heat Pipe, 12-Hour Radiation Cooled Test (Cryowall Off)	44

LIST OF FIGURES (Contd)

FIGURE		PAGE
21.	Axial Temperature Profile of the Planar Heat Pipe Compared Compared to Copper and Aluminum Fins, 5 Watts, One Hour Forced Convection Cooled Tests, No Preheat	45
22.	Axial Temperature Profile of the Planar Heat Pipe Compared to Copper and Aluminum Fins, 12 Watts, One Hour Forced Convection Cooled Tests, 5 Watt Hours Preheat	46
23.	Axial Temperature Profile of the Planar Heat Pipe Compared to Copper and Aluminum Fins, 20 Watts, One Hour Forced Convection Cooled Tests, 17 Watt Hours Preheat	47
24.	Transient Thermal Response for Planar Heat Pipe and Copper Fin for 20 Watt, -50°F Radiation Heat Sink Test	48
25.	Heat Pipe and Copper Fin Temperature Profiles for 12 Hour Radiation Cooled Test (Cryowall Off)	49
26.	Planar Heat Pipe Equilibrium Temperature Gradients, Forced Convection Cooling and 32 Grams H_2O, 12, and 20 Watts	59
27.	A Comparison of Experimental Convective and Boiling Film Heat Transfer Coefficients	62

LIST OF TABLES

TABLE		PAGE
I	Wick Friction Factor ($1/ft^2 \times 10^{-8}$) for Various Materials	9
II	Thermocouple Calibration for Planar Heat Pipe Experiment	24
III	Axial and Radial Temperature Gradients for Various Amounts of Working Fluid and Applied Power, Forced Correction Cooling, Near Horizontal Position	38
IV	Internal Temperature Measurements for Planar Heat Pipe During Radiation Cooled Tests, 32 gms H_2O, Near Horizontal Position	43
V	Power Settings and Measurement Error	52
VI	Internal Temperature Measurements for Planar Heat Pipe in Near Horizontal Position, Forced Convection Cooled	54
VII	Internal Temperature Measurements for Planar Heat Pipe in Vertical Position, Forced Convection Cooled	55
VIII	Comparison of Condenser Thermocouple and Pressure Transducer Measurements, Near Horizontal Position, Forced Convection Cooled	56
IX	Comparison of Condenser Thermocouple and Pressure Transducer Measurements, Vertical Position, Forced Convection Cooled	57
X	Mean Thermal Resistance Calculations for Planar Heat Pipe, Forced Convection Cooled Tests	60
XI	Comparison of Axial and Radial Temperature Gradients, Forced Convection and Radiation Cooled Tests	61
XII	Capillary Properties of Screen Wicks	64

LIST OF SYMBOLS AND CONVERSION FACTORS

A	area (cm^2 or in^2)
a	channel half-width (cm or in)
b	channel width (cm or in), $b = 2a$
g	gravitational constant (980.6 cm/sec^2 or 32.17 ft/sec^2)
h	height above arbitrary datum (cm or in)
$\bar{h}$	film heat transfer coefficient (BTU/hr ft^2 °F)
h_{vl}	heat of vaporization of liquid (cal/gm or BTU/lb)
k	thermal conductivity (watt/cm °C or BTU/hr in °F)
k_r	thermal conductivity of composite material (watt/cm °C or BTU/hr in °F)
κ_l	wick friction factor (per ft^2)
ΔL	length (cm or in)
l_m	maximum rise height of liquid in capillary (cm or in.)
m	mass (gm or lb_m)
$\dot{m}$	mass flow rate (gm/sec or lb_m/hr)
p	pressure (dynes/cm^2 or psi)
Δp	pressure gradient (dynes/cm^2 or psi)
$\dot{Q}$	heat transfer rate (watts or BTU/hr)
R, r	radius of curvature of liquid in capillary
R_T	thermal resistance (°C/watt or °F/BTU/hr)
T	temperature (°C or °F)
T_{tc}	temperature as measured by thermocouple (°C or °F)
T_p	temperature correlation of vapor pressure measurement (°C or °F)
T_o	ambient temperature (°C or °F)
T_i	mean internal temperature, $\frac{T_{ie} + T_{ic}}{2}$

LIST OF SYMBOLS AND CONVERSION FACTORS (Contd)

T_{ie}	evaporator internal temperature (°C or °F)
T_{ic}	condenser internal temperature (°C or °F)
ΔT_{er}	evaporator radial temperature gradient (°C or °F)
ΔT_{cr}	condenser radial temperature gradient (°C or °F)
ΔT_{ax}	mean axial external temperature gradient, evaporator to condenser (°C or °F)
ΔT_i	internal temperature gradient, $T_{ie} - T_{ic}$ (°C or °F)
u_o, u_o^*	vapor injection and condensation velocity (cm/sec or ft/sec)
V	volume (cm^3 or $in.^3$)
v'	void volume (cm^3 or $in.^3$)
V_L	volume flow rate (cm^3/sec or ft^3/hr)
X_T	total channel length (cm or in.)
x, y, z	cartesian coordinates

Subscript Notation

c	condenser
e	evaporator
i	internal
l	liquid phase or property
v	vapor phase or property

Greek Symbols

δ	capillary thickness (cm or in.)
ξ	porosity (%)
μ	viscosity of liquid or vapor (poise)
ρ	density (gm/cm or $lb_m/in.^2$)
σ	liquid surface tension (dynes/cm^2)

LIST OF SYMBOLS AND CONVERSION FACTORS (Contd)

Conversion Factors

length	1 cm = 0.3937 in. = 3 281 x 10^{-2} ft
area	1 cm^2 = 0.1550 $in.^2$ = 1.073 x 10^{-3} ft^2
volume	1 cm^3 = .06102 $in.^3$ = 3.531 x 10^{-5} ft^3
mass	1 gm = 2.205 x 10^{-3} b_m
density	1 gm/cm^3 = 3.613 x 10^{-2} $lb_m/in.^3$ = 62.43 lb/ft^3
energy	1 calorie = 3.968 x 10^{-3} BTU
pressure	1 $dyne/cm^2$ = 1.450 x 10^{-5} $lb/in.^2$
power	1 wat. = 1 joule/sec = 3.412 BTU/hr
viscosity	1 poise = $lgm/sec\ cm$ = 241.9 $lb_m/hr\ ft$

SECTION I

INTRODUCTION

This investigation was conducted to determine heat transport characteristics of a planar heat pipe. Heat pipes have been explored and employed for many aerospace uses, ranging from cooling cryogenic sensors to heat transfer devices for nuclear space power systems.

The planar heat pipe is potentially attractive as a passive temperature control device for advanced, large capacity, 20 to 100 ampere-hour (A-h) Nickel-Cadmium batteries. To date, very little data has been published on the performance of a planar heat pipe in the operational temperature regime (32-120°F) of such batteries. To explore the heat pipe's ability to provide battery cooling, a planar heat pipe using water as a working fluid was fabricated and tested. Battery waste heat was simulated by electrical heaters.

During battery discharge, heating occurs due to internal resistance and other loss mechanisms, which increases the temperature of the individual cells. Since the composite thermal conductivity of an individual sealed cell is extremely low (References 1, 2), typically 1/100 that of pure copper, cell temperature must be controlled by some means other than natural cell-to-cell conductive heat transfer. Battery (cell) performance and life are strongly dependent on cell temperature (References 2,3). For maximum life, cell temperatures should be maintained between 40-80°F (Reference 3).

Typical spacecraft and aircraft batteries are composed of groups of individual rectangular cells in a box-like configuration. Cooling must be provided for the cell stack, and the rejected waste heat must be transported to the vehicle heat exchanger (e.g., space radiator or forced convection blower).

To minimize charge control imbalance due to thermal effects and maximize battery efficiency, a variety of cooling techniques have been proposed, including intercell metallic conduction straps and pump-driven fluid heat exchangers. For the high power (1-10 kw) batteries envisioned for future aerospace vehicles, metallic-conduction-strap cooling may not be adequate to provide uniform cell

temperature. For space missions of greater than a few years duration, pump life may preclude using a circulating fluid heat exchanger to cool the battery. Thus, the heat pipe might prove to be the most practical and effective device to provide battery cooling for both spacecraft and aircraft.

This investigation was limited to exploring the heat pipe as a means of intercell cooling--that is, cooling two adjacent rectangular cells of a battery stack with a heat pipe of planar geometry to maximize the heat transfer area. The working fluid was high purity water. Battery waste heat was simulated by electrically heated copper blocks. External axial temperature distributions along the planar heat pipe were measured as were internal evaporator and condenser temperatures and working fluid vapor pressure. Forced convection and in-vacuum radiation cooling tests were conducted. Testing with an actual battery was beyond the scope of this effort.

SECTION II

THEORY OF PERFORMANCE

1. THE HEAT PIPE

The heat pipe is a simple, self-contained, heat transfer device which exhibits an effective thermal conductivity exceeding any known homogeneous material (Reference 4). This high thermal conductance is achieved by transferring heat via evaporation and condensation of a fluid within a wick-lined pressure vessel. The fluid (termed working fluid) evaporates at one end of the device, differential pressure carries the vapor with the heat of vaporization to another section, where the vapor condenses and the heat is rejected. The fluid is returned to the evaporator via wick force (capillary pumping). The heat pipe is closely analogous to the ordinary steam heating radiator system, where the wick serves as the liquid return mechanism rather than gravity.

Within certain limits, the heat pipe is capable of transferring heat energy from one point to another with very small temperature differences. The principles of surface chemistry, heat transfer, and fluid mechanics govern its performance; these principles are described in the following paragraphs.

2. FUNDAMENTAL CAPILLARY PHYSICS

The phenomenon of capillarity has been examined extensively in the study of surface chemistry. The flow of liquid through a capillary structure is the fundamental physical mechanism governing heat pipe operation.

a. The Law of Laplace and Young

Liquid surface tension forces exist at the interface of a solid, liquid, and energy interaction of the surface and subsurface liquid molecules and the molecules of the surrounding vapor of solid container material (Reference 5). Surface tension forces give rise to the observed capillary tube meniscus; the shape of the meniscus is determined by the relative strengths of liquid intermolecular cohesive forces as compared to the intermolecular adhesive forces on the liquid due to the container walls.

Young and Laplace, in 1805, developed the basic equation of capillarity. The equation relates the pressure drop, Δp_l, across a curved liquid/vapor interface surface to the surface tension, σ, of the liquid (Reference 7). The Laplace-Young equation is given by

$$\Delta p_l = \sigma \left(\frac{1}{R_1} + \frac{1}{R_2} \right) \tag{1}$$

where R_1 and R_2 are the radii of curvature defining the surface under consideration. Notice for a flat liquid/vapor interface, $R_1 = R_2 = \infty$ and $\Delta p_l = 0$. For a hemispherical surface, i.e., $R_1 = R_2$, and the Laplace-Young equation reduces to

$$\Delta p_l = \frac{2\sigma}{R} \tag{2}$$

The liquid surface tension appearing in the above equations may be interpreted as the "surface-free energy/unit area" or the "force/unit length" which prevents the surface interface from fluctuating and/or expanding.

b. The Capillary Pump

The phenomenon of capillary pumping of a liquid by the wick (porous solid or capillary structure) is fundamental to heat pipe operation. The capillary pumping or wicking forces must overcome the frictional and gravitational forces, where present, to provide continuous liquid return flow. To examine the mechanism of capillary pumping, a simplified one-dimensional model of the planar heat pipe will be considered, after Kunz, Langston, Hilton, Wyde, and Nashick (Reference 8).

Figure 1 illustrates this simplified model. In the equations to follow, the pressure will be denoted by p, with subscripts l, v, e, and c referring to the liquid, vapor, evaporator, and condenser, respectively. Consider the net flow of vapor and liquid in the device and the local vapor and liquid pressures at arbitrary, but fixed, stations of the evaporator and condenser. If the heat pipe is to operate, there must be vapor flow from the evaporator to the condenser, and liquid flow from the condenser to the evaporator. In order for liquid to flow from the condenser to the evaporator, pressure in the condenser must be

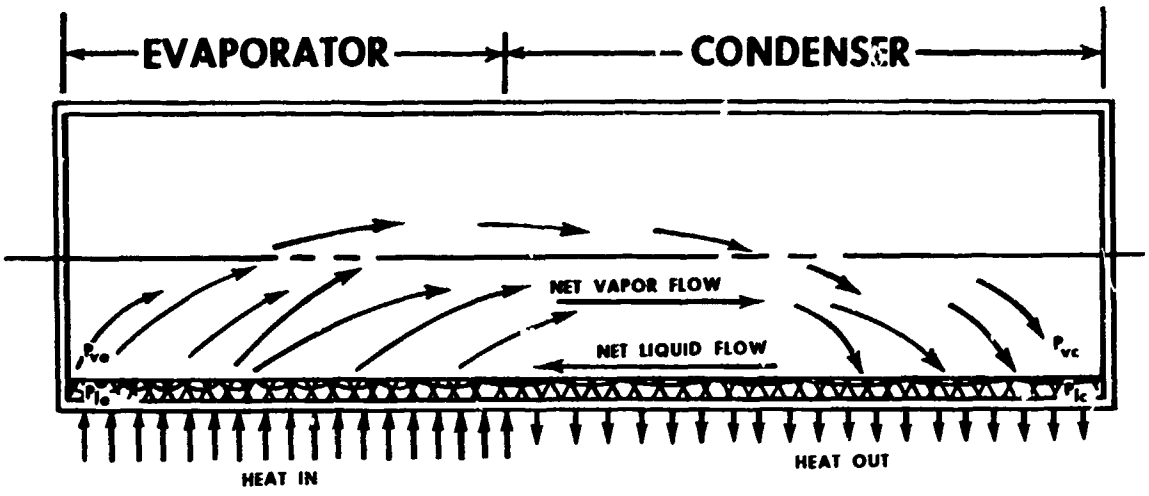

Figure 1. Two-Dimensional Model of Planar Heat Pipe

greater than that in the evaporator, so as to cancel liquid friction losses and momentum changes. Thus,

$$(p_l)_c \geq (p_l)_e \tag{3}$$

Simarily, for vapor to flow from the evaporator to the condenser

$$(p_v)_e \geq (p_v)_c \tag{4}$$

Requirements for steady operation may be determined by summing the pressure changes incurred by a given fluid "particle" as it leaves the evaporator, condenses, and returns. This summation must, of course, be zero for equilibrium flow. Therefore,

$$\left[(p_v)_e-(p_v)_c\right]+\left[(p_v)_c-(p_l)_c\right]+\left[(p_l)_c-(p_l)_e\right]+\left[(p_l)_e-(p_v)_e\right]=0 \tag{5}$$

We may combine the pressure decreases due to friction and rate change of momentum as

$$\left|(\Delta p)_D\right| = \left|\left[(p_v)_e-(p_v)_c\right]+\left[(p_l)_c-(p_l)_e\right]\right| \tag{6}$$

where, in general,

$$\left|\Delta p_D\right| > 0 \tag{7}$$

At any vapor/liquid interface, the pressure change across the interface is given by the Laplace-Young Equation of Capillarity, Equation 1. Assuming that the condenser and evaporator interfaces can be characterized by a single radius of curvature, R_e and R_c, respectively, Equation 2 applies, and the pressure changes at the vapor-liquid boundary in Equation 5 are given by

$$(p_v)_c - (p_l)_c = \frac{2\sigma}{R_c} \tag{8}$$

$$(p_l)_e - (p_v)_e = \frac{2\sigma}{R_e} \tag{9}$$

If the variation in surface tension, σ, with temperature may be neglected, Equation 5, through substitution with Equations 6, 8, and 9, becomes

$$(\Delta p)_D = \frac{2\sigma}{R_e} - \frac{2\sigma}{R_c} \tag{10}$$

Equating Equations 7 and 10 gives

$$\left|(\Delta p)_D\right| = \left|\frac{2\sigma}{R_e} - \frac{2\sigma}{R_c}\right| > 0 \tag{11}$$

Mathematically, Equation 11 requires that

$$R_e < R_c \tag{12}$$

Physically, Equation 11 may be interpreted as the magnitude of the capillary force/unit area under equilibrium vapor and liquid flow conditions. Stated differently, the capillary pump (wick) overcomes frictional and inertial forces in the liquid by forming a larger radius of curvature at the condenser than at the evaporator.

The wick may be considered a homogeneous porous structure capable of supporting multiple fluid levels. When vapor production is minimum (minimum heat input), wick fluid level is maximum. Conversely when wick fluid level is minimum, vapor production is maximum. When vapor production is high, the vapor/liquid interface retreats into the interior of the wick, and capillary pumping occurs internal to the apparently "dry" wick surface.

The net capillary force over the entire device is obtained, in principle, by integrating over all the pore sites and sizes to obtain the average capillary pressure. Mathematically this is impossible for most complex wick structures, and capillary pumping forces must be measured experimentally.

c. Fluid Flow in Porous Media/Darcy's Law

The theory of liquid flow and pressure losses through a homogeneous porous media are based on the experimental observations made by H. Darcy in 1865 (Reference 9). As illustrated in Figure 2, Darcy's experiment consists of a homogeneous capillary filter bed of height, h, and uniform cross sectional area, A, where $h = Z_2 - Z_1$. The filter bed is equipped with inlet and outlet ports, and open manometers, at height Z_1 and Z_2, to measure pressure drop due to liquid flow through the bed. The liquids in the manometer rise to heights h_2 (upper or inlet manometer) and h_1 (lower or outlet manometer), respectively. From the Navier-Stokes and continuity equations, one may deduce the following equation, known as Darcy's Law

$$V_l = -\frac{KA(h_2 - h_1)}{h} \tag{13}$$

where K is a constant of the porous medium and the fluid. The volume flow rate of the liquid, V_1, is given by

$$V_l = A\,u_l = \frac{\dot{m}_l}{\rho_l} \tag{14}$$

where u_1 is the liquid velocity, $\dot{m}_1$ is the liquid mass flow rate, and ρ_1 is the liquid density.

An alternate form of Darcy's Law can be written in terms of the pressures and liquid density,

$$V_l = \frac{K'A}{h}\left[(p_2 - p_1) + \rho_l\, gh\right] \tag{15}$$

where K' is the redefined constant

$$K' = \frac{Kh}{\rho_l g} \tag{16}$$

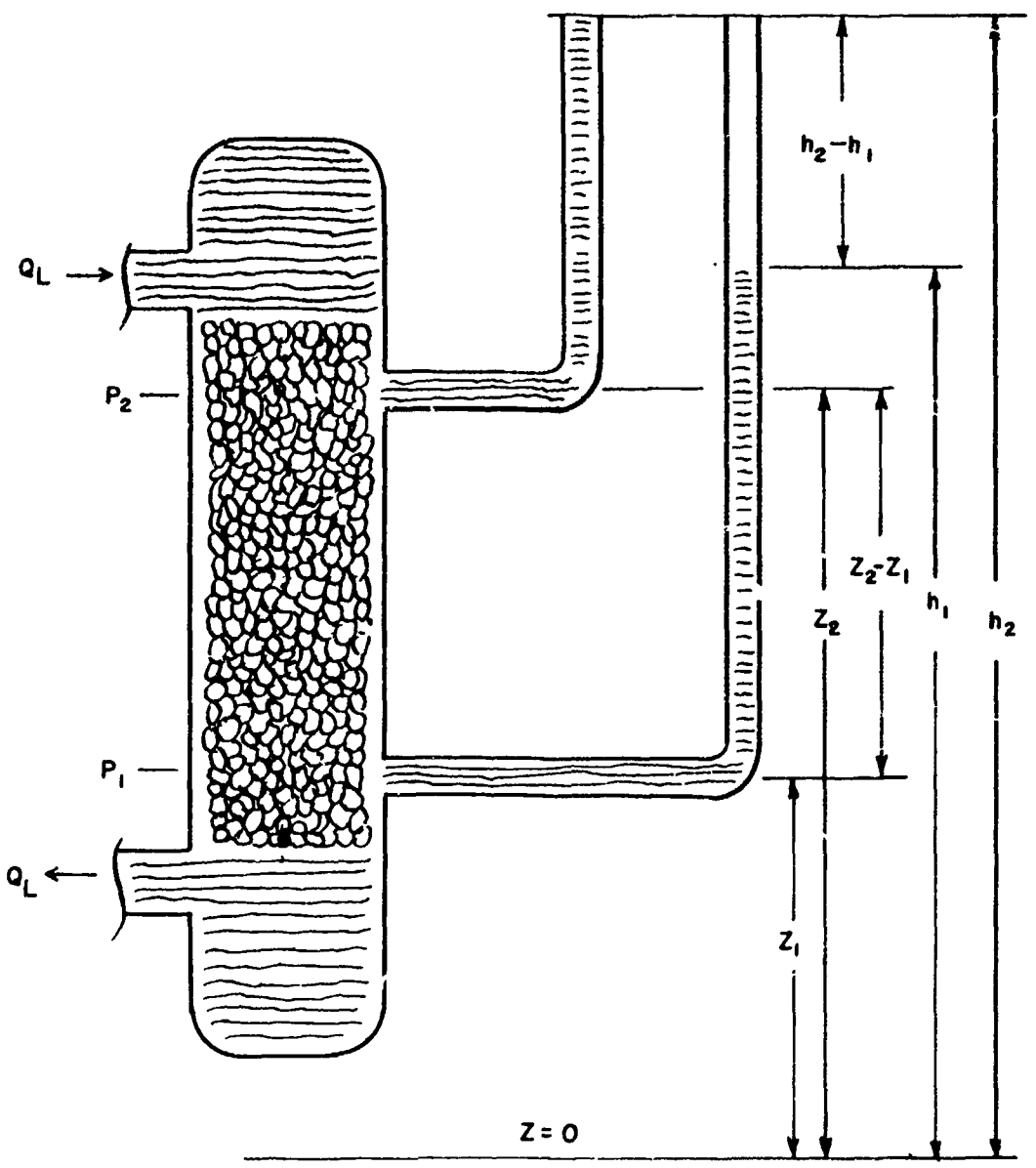

Figure 2. Darcy's Experiment

Equation 15 can be written in differential form such that

$$V_l = -K' A \frac{dp_l}{dx} \tag{17}$$

Rearranging Equation 17 and redefining constants gives a pressure gradient for a liquid flowing in a porous structure

$$\frac{dp_l}{dx} = -\frac{\dot{m}_l}{A}\left(\frac{\mu_l}{\rho_l}\right) K_l \tag{18}$$

where μ_1 is the liquid viscosity and the constant K_1 is the reciprocal of permeability, termed the "wick friction factor." K_1 is independent of the fluid properties, and depends only on the physical structure of the wick. The relationship between K', K_1, and μ_1 is deduced from dimensional analysis and proven by experiment. In general, K_1 must be determined experimentally due to the complex geometry of the capillary pore structure and interconnects. Table I lists some values of wick friction factors for various materials (References 10, 11).

TABLE I

WICK FRICTION FACTOR ($1/FT^2 X10^{-8}$) FOR VARIOUS POROUS MATERIALS

Material	K_1 (per ft^2)
Fiber glass	$18x10^8$-$39x10^8$
Soil	$66x10^8$-$3200x10^8$
Hair Felt	$0.77x10^8$-$1.1x10^8$
Cigarette	$0.64x10^8$
Multilayer 50 to 200 Mesh Screen	1.4-$12x10^8$
Sintered Metal Fibers	$0.80x10^8$-$61.7x10^8$
Sintered Metal Powders	$3.1x10^8$-$11.5x10^8$

3. VAPOR FLOW IN A RECTANGULAR CHANNEL

The viscous pressure losses in a vapor flowing in a rectangular channel may be determined analytically by solving approximations to the Navier-Stokes equations. The heat transfer occurring in the evaporator and condenser sections of the channel may be considered by incorporating the appropriate boundary conditions.

Knight and McInteer (Reference 12) reduce the problem of vapor flow in a rectangular channel by considering two-dimensional laminar flow with uniform injection (evaporation) and suction (condensation) at the channel walls. This formulation results in a third-order nonlinear differential equation which can be solved only by computer integration. For a low viscosity vapor such as water, however, the equation may be simplified and integrated directly. The axial pressure drop reduces to

$$\left.\frac{dp}{dx}\right|_{evap} = -\frac{\pi}{2}\frac{\rho_v \mu_0}{a^2} x \tag{19}$$

in the evaporator, and

$$\left.\frac{dp}{dx}\right|_{cond} = -\frac{\rho_v \mu_0^{*2}}{a^2} x^* \tag{20}$$

in the condenser, where a is the channel half-width, μ_0 and μ_0^* are the vapor evaporation and condensation velocities, and x and x* are the axial position coordinates in the evaporator and condenser, respectively.

For the planar heat pipe, in the temperature and input heat flux range of interest, the axial pressure loss due to vapor viscosity is extremely small compared to the vapor pressure of water. The calculations shown in Appendix I verify that the vapor pressure in the heat pipe is essentially constant over the entire length (see Appendix I).

4. VAPOR GENERATION AND CONDENSATION IN CAPILLARY WICK

The process of vapor production and condensation is of interest in the design of a heat pipe. The input heat is conducted through the heat pipe's metallic wall

to the capillary wick and the liquid. As the temperature of the liquid and wick increases, the rate of evaporation at the liquid-wick-vapor interface increases. Three distinct regimes of vaporization exist (Reference 13). At low heat fluxes, vapor is generated at the surface of liquid-wick-vapor interface via natural heat convection and conduction through the liquid-saturated wick. For higher heat fluxes, nucleate boiling occurs at the wall-wick-liquid interface, when locally superheated liquid forms small vapor bubbles which are convected through the wick and escape into the vapor space. Finally, film boiling occurs at very high fluxes, which forms a layer of low-thermal-conductivity vapor at the wall-liquid-wick interface and causes the wall temperature to rise excessively.

For low heat fluxes, assuming thermal conduction as the mechanism of vapor production, Gorring and Churchill show that heat transferred, $\dot{Q}$, through the homogeneous liquid-saturated wick is given by (Reference 14)

$$\dot{Q} = (k_T)\, A\, \Delta T = \frac{k_w}{1+\epsilon\left(\frac{k_w}{k_l}-1\right)}\, A\, \Delta T \qquad (21)$$

where k_l and k_w are the thermal conductivity of the liquid and the capillary wick, respectively, k_T is the effective thermal conductivity of the composite medium, ϵ is the porosity of the wick, A is the heat transfer area, and ΔT is the temperature drop through the wick.

If natural convection or nucleate boiling is the mechanism of vapor production, the temperature drop through the liquid is given by

$$\Delta T = \frac{1}{\bar{h}}\ \frac{Q}{A} \qquad (22)$$

where Q/A is the input power and $\bar{h}$ is the film or boiling heat transfer coefficient.

For low input power flux, $\bar{h}$ is of the order of 60 BTU/hr ft^2°F for water evaporating from a heated flat plate at atmospheric pressure (Reference 15). It should be noted that $\bar{h}$ is a function of pressure (Reference 16).

5. ANALYTICAL MODEL OF PLANAR HEAT PIPE

Kunz, et al, combine the equation of fluid mechanics (force, continuity, and energy) with the equations of capillary pumping (capillary force, viscous liquid pressure loss) and heat transfer (vaporization and condensation) to describe the performance of a vapor chamber fin, or planar heat pipe (Reference 17). Their analysis shows the maximum heat transfer rate is

$$Q_{max} = 2b\delta\left(\frac{\rho_l h_{vl} \sigma}{\mu_l}\right)\frac{\sigma}{K_l R_{min} X_T} \tag{23}$$

where b is the channel width, ρ_l the liquid density, μ_l the liquid viscosity, h_{vl} the latent heat of vaporization of the liquid, σ the liquid surface tension, δ the wick thickness, K_l the wick friction factor, R_{min} the minimum radius the capillary can support, and X_T the total length of the channel or heat pipe.

Since it is difficult to calculate or actually measure R_{min}, Kunz, et al, suggested a practical experimental technique to determine effective R_{min}. By measuring the maximum vertical height that the liquid rises in the capillary against a 1.0g gravity field and relating this height to the elementary hydrostatic pressure equation and the Laplace-Young Law, the effective R_{min} for the entire capillary wick is

$$(R_{min})_{eff} = \left(\frac{2\sigma}{\rho_l g l_m}\right)_{wR} \tag{24}$$

where l_m is the observed height of the fluid in the capillary, and the subscript wR denotes wick rise test conditions; R and σ are based on the temperature at which the wick rise tests were conducted.

Substituting Equation 24 into Equation 23, the expression for the maximum heat transport rate in the planar heat pipe becomes

$$Q_{max} = 2\left(\frac{\rho_l h_{vl} \sigma}{\mu_l}\right)\left(\frac{b\delta}{X_T}\right)\left(\frac{g\rho_l}{\sigma}\right)_{wR}\frac{l_m}{K_l} \tag{25}$$

Appendix III shows the calculation of Q_{max}, which is termed burnout heat flux, for the planar heat pipe based on the results and data described in Sections IV and V.

SECTION III

DESCRIPTION OF EXPERIMENTS AND APPARATUS

1. APPROACH

Several conventional cylindrical heat pipes and a prototype planar heat pipe were fabricated and tested. These devices are shown in Figure 3.

Initial tests were conducted on a cylindrical Pyrex (tubing) glass heat pipe having nominal dimensions of 1.2 cm diameter and 12 inches length. The pipe was lined with three layers of 100-mesh stainless steel (60% dense, .0045 wire diameter) capillary material. A brass to rubber O-ring seal and fill valve were attached so that the amount of working fluid could be varied.

A cylindrical stainless steel pipe 1 inch in diameter and 12 inches long was then fabricated and tested. The pipe was instrumented internally with four #36 copper-constantan thermocouples and externally with seven #24 copper-constantan thermocouples. These devices contributed valuable information on basic fabrication, cleaning, loading, and testing procedures; they performed in a nearly isothermal manner, which lent confidence to the planar heat pipe development. The remainder of this report will describe only those aspects of the experimental work related to the planar heat pipe.

2. PLANAR HEAT PIPE CONFIGURATION, MATERIALS, AND FABRICATION

The initial consideration in designing the planar heat pipe was its size; we decided to scale it to the size of experimental 20 A-h nickel cadmium cells being tested by the Air Force Aero Propulsion Laboratory. These cells are flat and rectangular, and measure approximately 1 inch by 3-1/2 inches by 6 inches. The planar heat pipe was designed to cool the largest flat surface of the cell, i.e., the 3-1/2-inch by 6-inch face. The condenser section was made the same size as the evaporator. For ease of fabrication, 1/2 inch was selected as the width dimension. Thus, the overall dimensions were 1/2 x 3-1/2 x 12 inches.

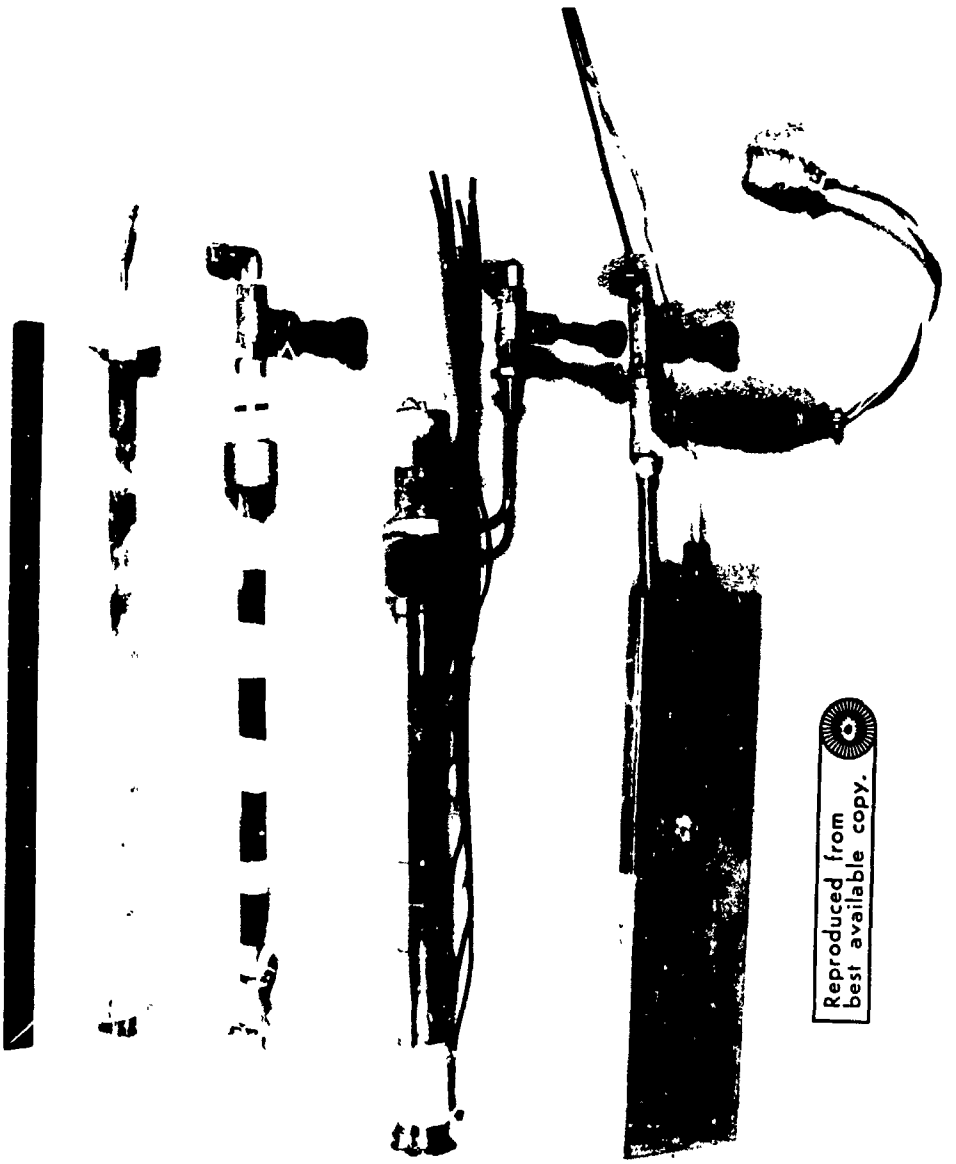

Figure 3. Several Experimental Heat Pipes

Water was selected as the working fluid since a relative abundance of thermophysical data (vapor pressure, density, viscosity, surface tension, heat of vaporization) is available in the temperature regime of interest.

The outer shell of the planar heat pipe was fabricated from .025" sheet, Type 304, stainless steel. The capillary material consisted of two layers of 100-mesh, Type 304, stainless steel screen. The manufacturer's specification stated the screen density was 60%, with .0045-inch wire diameter. Thickness of a single layer of screen was measured to be .010 ± .002 inches.

The outer stainless steel shell was fabricated on a flat last, with the seam soft-soldered. Two end caps were fabricated, and one was soft-soldered into place on the stainless steel shell. The capillary screen material was wrapped on a 3/8-inch-thick rectangular Plexiglas last, inserted into the shell, and the last withdrawn.

A pipe 1/2 inch in diameter by 11 inches long, made of Type 304 stainless steel with a 3/32-inch wall thickness, was filed flat on opposite sides to reduce the outside diameter slightly. This pipe was inserted into the heat pipe to serve as an antibuckling structural member, since the heat pipe operates at less than 1 atmosphere internal pressure. Two inconel wire loops were soldered to the pipe and bent so as to spring-load two #24 gauge copper constantan thermocouples against the screen liner when the flat-edged pipe was inserted into the wick-lined shell. After the pipe was inserted into the shell, four #24 gauge inconel springs were wound (1/2-inch diameter, 12-inch length, 4 turns per inch) and inserted in the shell to promote screen contact with the wall.

A condenser end plate was fabricated from .025-inch stainless steel, and two 3/8-inch holes were drilled in it to accommodate a connex coupling (thermocouple lead-through) and a strain gauge pressure transducer. A 3-inch length of 3/8-inch O.D. stainless steel pipe was silver-soldered on the condenser end cap to allow the pressure transducer and filling apparatus to be attached. The thermocouples were fed through a ceramic insert, and a Teflon seal in the connex fitting and the condenser end plate assembly was soft-soldered in place onto the rectangular shell. The assembled device was then electrochemically

plated with 3 mils of copper on the evaporator section to ensure good surface thermal conduction. External thermocouples then were attached by spot-welding. Figure 4 is a photograph of the assembled planar heat pipe. An assembly drawing of the device with pertinent dimensional and material information and thermocouple locations is shown in Figure 5.

3. CLEANING AND LOADING PROCEDURES

In order to prepare the heat pipe for testing, the assembly was first filled with trichloroethelyne to remove any residual greases and oils. It was emptied and filled with a 10% NaOH-distilled water solution to clean internal surfaces (Reference 18), and left to soak for 24 hours. It was then emptied, flushed immediately with preboiled, filtered, singly distilled, deionized, and demineralized water, evacuated by vacuum pumping through a water trap, reflushed with water, and re-evacuated to 10^{-5} mm Hg via the vacuum pumping system.

Working fluid was introduced into the evacuated pipe by employing the filling apparatus shown in Figure 6. Despite its complex appearance, the filling system is functionally very simple, as shown in the schematic diagram in Figure 7. Filtered, deionized water, which was boiled to remove absorbed oxygen, was transferred to a vacuum-evacuated, calibrated burette via a neoprene tube. The neoprene tube contained a plastic T section where the flow was split. The tube to the heat pipe was closed while the water filled the burette and heat pipe fill tube; then the supply tube was opened and the red amount of working fluid was metered into the heat pipe. A small nitro, overpressure had to be applied to the burette to transfer large amounts of working fluid.

The amount of working fluid was varied; 8, 16, 20, 24, 32, and 64 grams of water were introduced for the various tests. After filling, the device was resealed, removed from the filling apparatus, and readied for testing. The amount of water introduced could be controlled to about 0.10 gm.

After a test, the water was removed by vacuum pumping to 10^{-5} mm Hg. The device was then reloaded with the desired amount of water and tested. A Veeco MS-9 leak test console with both a mechanical fore pump and a liquid-nitrogen-cooled diffusion pump was used to evacuate the heat pipe. The water

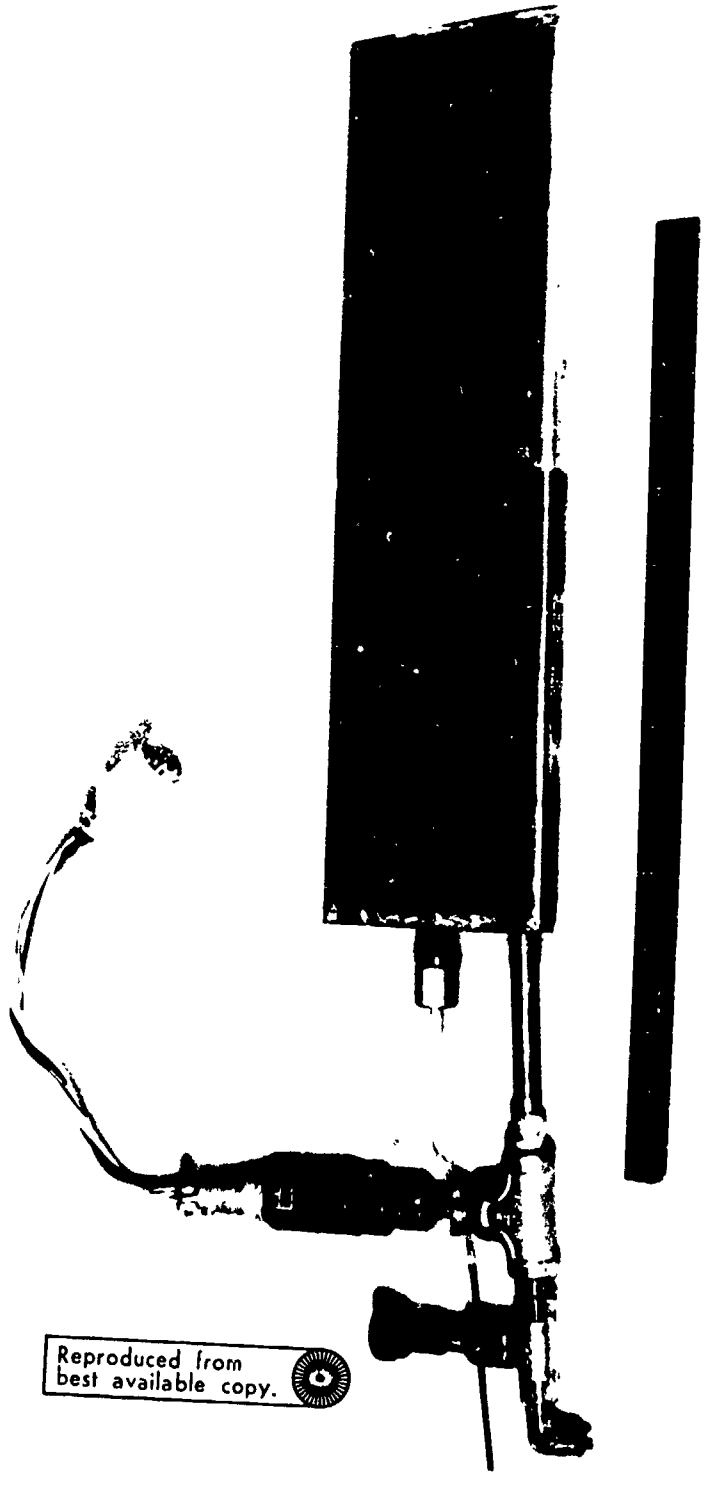

Figure 4. Assembled Planar Heat Pipe

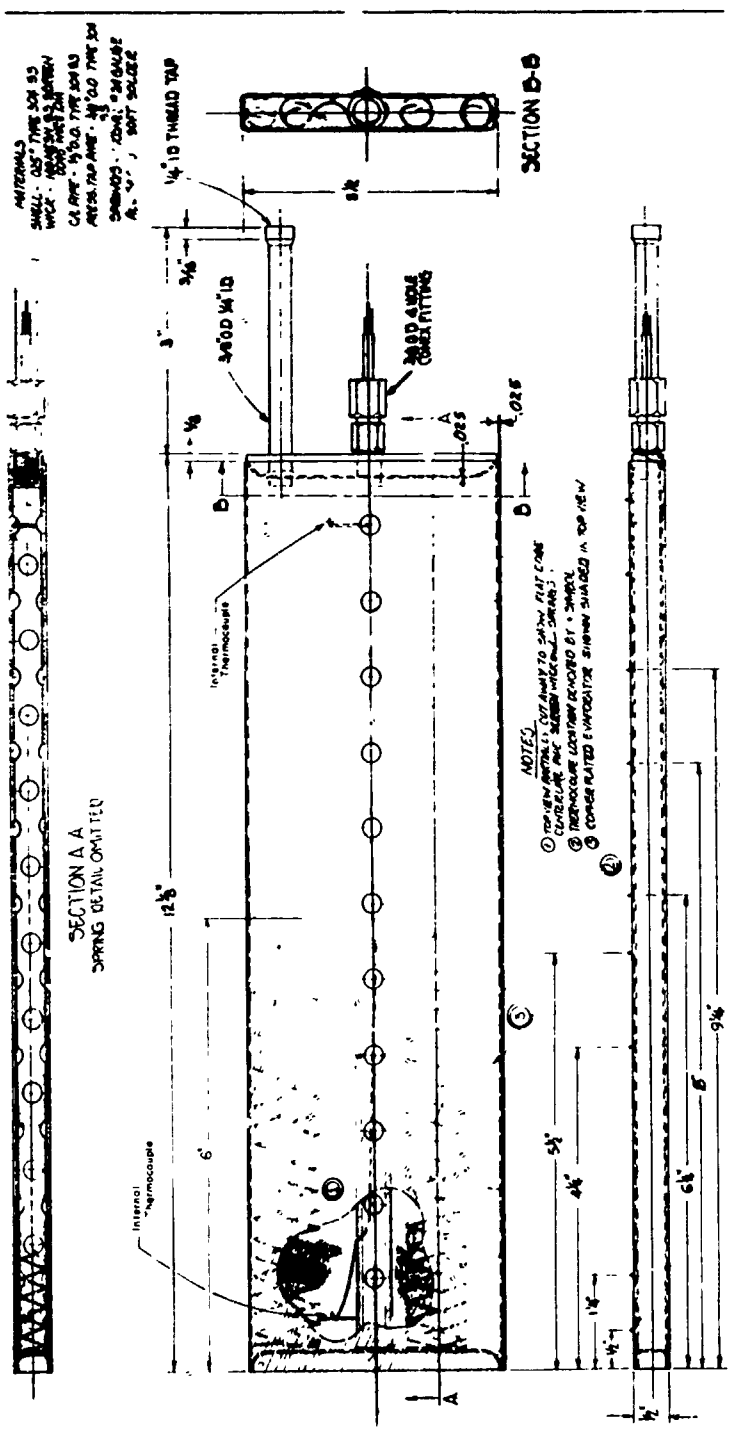

Figure 5. Assembly Drawing of Planar Heat Pipe

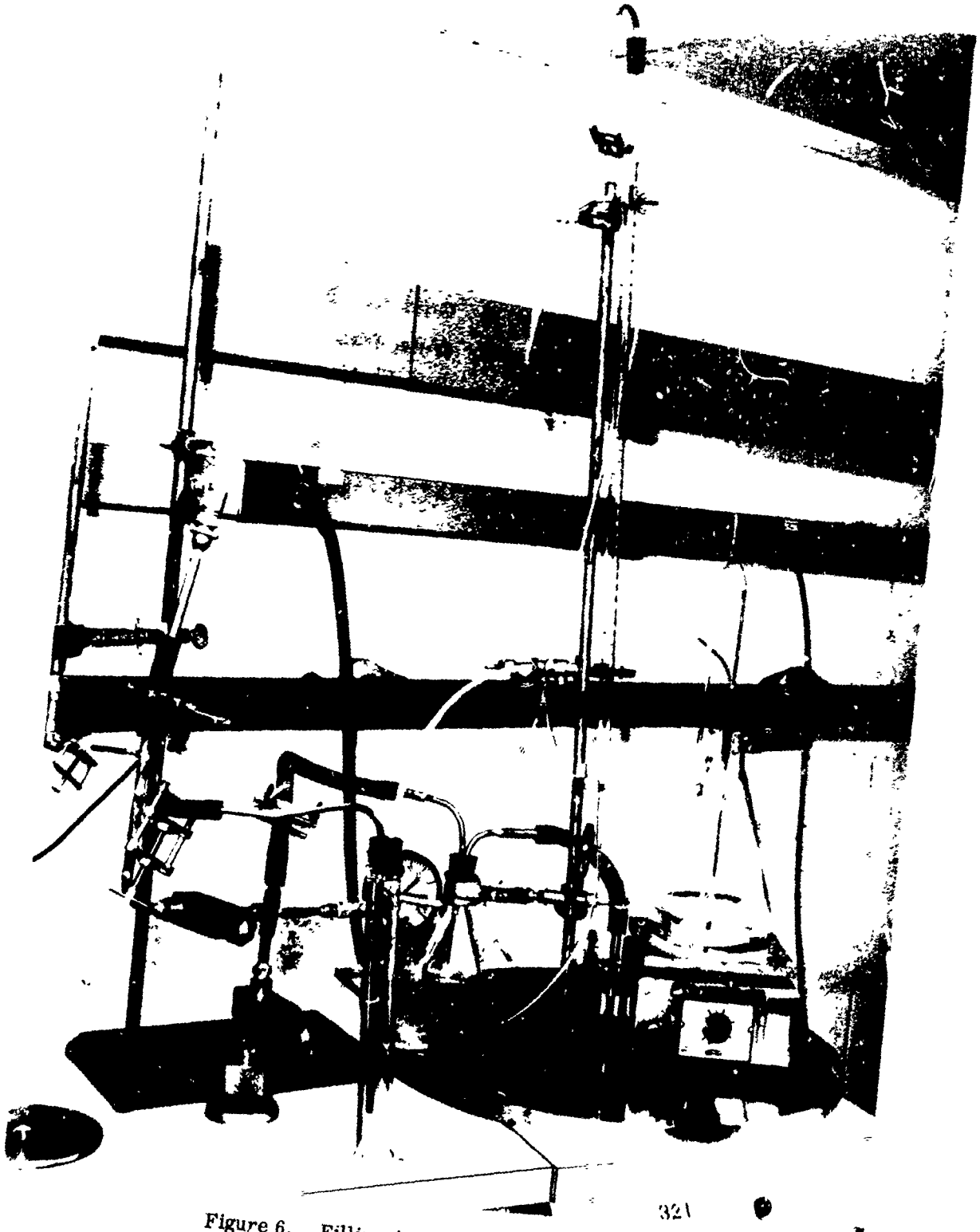

Figure 6. Filling Apparatus for Planar Heat Pipe

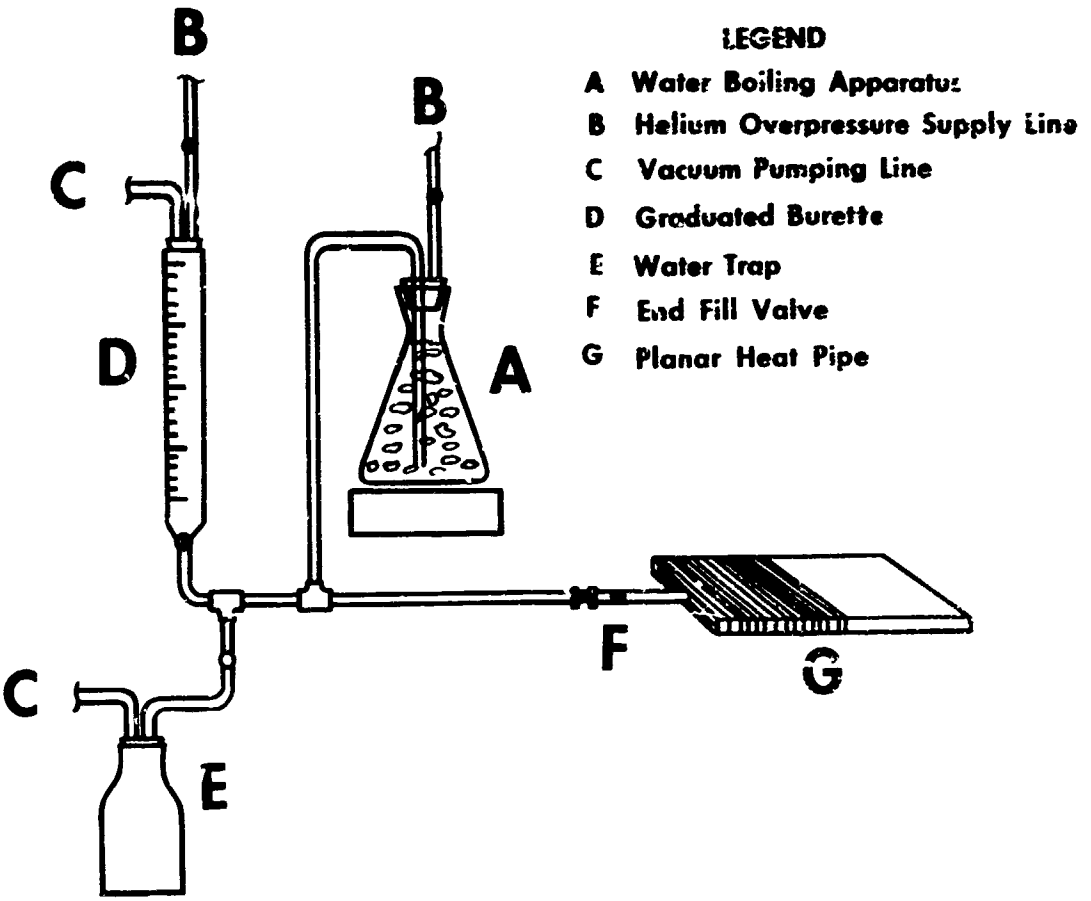

Figure 7. Schematic Diagram of Filling System

trap was employed to minimize water accumulation in the fore pump oil reservoir.

Leak checks were performed on both the planar heat pipe and the filling system, using a helium blowdown probe and a Veeco audio leak detector. Several small leaks in the heat pipe and loading apparatus were noted and corrected.

4. WORKING FLUID PREPARATION

In order to ensure high purity of the water used for the working fluid, we processed singly distilled water through a Millipore Corporation "Super-Q" Deionization/Filtration System. This three-step process provides prefiltration, organic absorption, and deionization of any chemical contaminants dissolved in the distilled water. Before loading the heat pipe, this high purity water was boiled to remove any residual atmospheric gases.

5. INSTRUMENTATION AND ELECTRICAL TESTING APPARATUS

Thermocouples were fabricated from #22 and #36 copper-constantan material. Two copper heater blocks, each 3/8 inch x 4 inches x 6 inches were employed to simulate the batteries. A nichrome ribbon heater was embedded on one side of the copper block, which had been coated with General Electric silicon rubber paste. The nichrome ribbon was folded in a laced, square-S pattern and placed on the silicon-coated copper. The assembly was recoated with silicon rubber, and a 1/16 x 4 x 6 inch phenolic cover plate was pressed on to seal the simulated batteries. Both copper heater plates were resistance-checked to ensure no current leakage from the nichrome ribbon to the copper.

Four #36 thermocouples were loaded in 1/32-inch slot cut into one of the copper blocks to measure external evaporator temperature, as shown in Figure 8. Two #36 copper-constantan thermocouples were installed internally, approximately 1/2 inch from each end of the heat pipe to measure internal evaporator and condenser temperatures (see Figures 4 and 5). These internal thermocouples were jacketed with Teflon shrink tubing to prevent shorting and spurious readings. Five #22 copper-constantan thermocouples were then

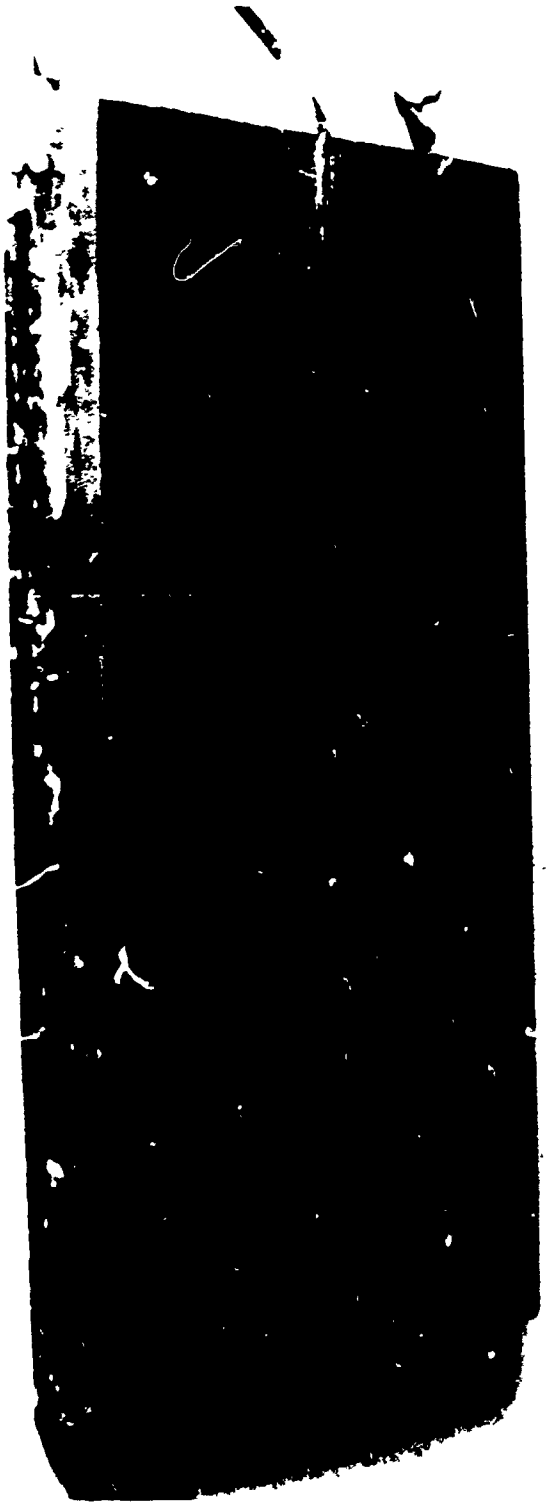

Figure 8. Copper Heat Source

spot-welded to the external condenser section. The locations of all 11 thermocouples are shown in Figure 4.

A Minneapolis-Honeywell Brown Electronic 12-channel recorder was used to record temperature measurements. This recorder operated in the -100°F to 200°F range, with a printing speed of one channel per second. The manufacturer guarantees a printing accuracy for the Brown Recorder of 0.25% full scale, or ±0.75°F. The manufacturer's guaranteed tolerance on the thermocouple wire is ±1.5°F. Thus, the maximum temperature sensing error is ±2.25°F.

To check the actual error, the Brown Recorder was first calibrated using a standard bridge milliwatt signal generator. The thermocouple/recorder printout was then compared to the digital readout of two Dymex Quartz Thermometers (Model 280/A) which had been calibrated to National Bureau of Standards specifications (±0.04°F from 32-212°F). Table II summarizes the thermocouple/printout calibration test conditions and error based on the quartz thermometers. The maximum error was 1.14°F, the minimum 0.01°F, and the mean 0.56°F. An error of less than ±1°F was considered acceptable for these experiments.

An additional check on the measured internal thermocouple temperatures was provided by a strain gauge pressure transducer to monitor vapor pressure. The Consolidated Electrodynamics Corporation (CEC) Type 4-326-0003, 0 - 10.0 psia range transducer was calibrated to the 0 - 2.0 psia range using a CEC Precision Pressure Controller Type 6-301-D100 calibration console. An applied test pressure was sensed by both the transducer and electromanometer system of the console. The electromanometer provided a digital display of the test pressure; the transducer output was fed into a Brown Potentiometer/Recorder (0-50 mv input signal). A pressure-millivolt signal output curve was generated in the 0 -2 psia range in 0.2 psia increments. Calibration of the transducer, based on this procedure, was 0.05% full scale, or ±0.001 psia. In practice, the calibration curve could be read accurately to about 0.01 psia. The pressure transducer calibration curve is shown in Figure 9.

After heat pipe assembly, loading, and instrument calibration, the copper heat plates were wired into place to ensure good thermal contact with the evaporator. The evaporator-heater plate section was wrapped with 1-1/2 inches

TABLE II

THERMOCOUPLE CALIBRATION FOR PLANAR HEAT PIPE

Test Description	T_{tc}* (°F)	T_{q1}* (°F)	T_{q2}* (°F)	ΔT_q (°F)	$\bar{T}_q$ (°F)	Error, $\bar{T}_q - T_{tc}$ (°F)
Water, Ice Bath	32.0	32.0	32.26	.26	32.13	+.13
Water, Room Temp.	73.2	73.18	73.24	.06	73.21	+.01
Water, Room Temp.	73.1	73.08	73.35	.33	73.16	+.06
Water, Hot	160.0	160.75	160.39	.36	160.57	+.51
Water, Hot	159.0	159.42	159.53	.09	159.46	+.46
Water, Warm	119.5	120.24	120.76	.52	120.50	+1.0
Water, Warm	110.0	111.03	111.25	.22	111.14	+1.14
Water, Warm	100.9	101.59	101.93	.44	101.78	+.89
Forced Air	75.6	76.48	76.48	0	76.48	+.48
Forced Air	75.2	75.74	75.24	.49	75.44	+.29
Forced Air	78.3	79.25	79.04	.16	79.17	+.43
Forced Air	76.8	77.66	77.00	.47	77.83	+1.03
Forced Air	77.7	77.59	77.52	.07	77.55	-.15
Forced Air	79.4	80.27	79.81	.36	79.99	+.55
Forced Air	80.0	80.78	81.08	.30	80.93	+.93

*T_{tc} - Thermocouple temperature readings

T_{q1}, T_{q2} - Quartz thermometer temperature readings

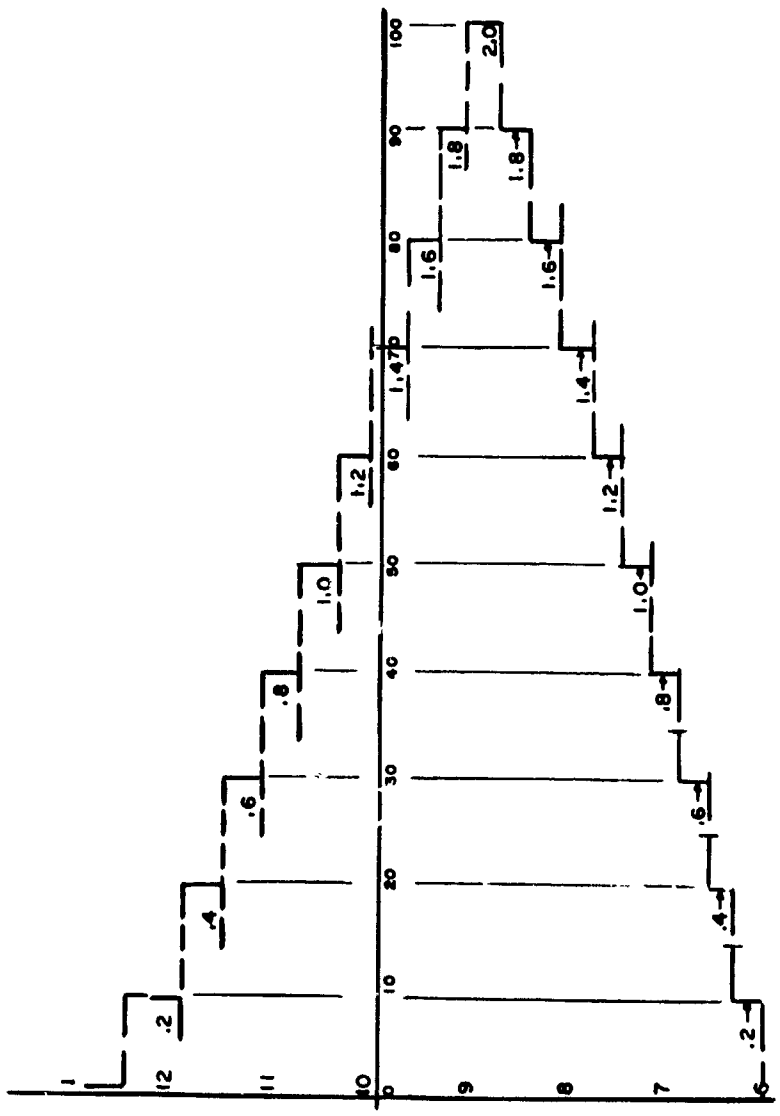

Figure 9. Pressure Transducer Calibration Curve

of Carborundum "Fiberfrax" ceramic fiber insulation to minimize evaporator heat losses. The device was held at the evaporator end by a chain and laboratory stand, as shown in Figure 10. Copper power leads (#12 copper wire) were clipped onto the nichrome heater ribbon tabs. Electrical power was supplied by a Trygon Electronics DC Power Supply, Model HR 40-3B, 0 - 40v, 0 - 3A. Current was measured with a precalibrated Weston-Ammeter Model 741, No. 8389 ±1% full scale accuracy. Voltage was measured at the nichrome tab clip lead junction with a Weston Voltmeter, Model 901, No. 608, ± 0.5% full scale accuracy, 0 - 15v. For the tests in vacuum, the plates were coated with Dow Corning thermal grease to ensure good contact with the evaporator.

6. TEST DESCRIPTION

a. Forced Convection Cooled Tests

The device was placed on a laboratory clean bench station, and a blower unit was used to provide a uniform flow of low-velocity room-temperature air to cool the condenser section of the pipe. The 1/2-inch edge of the heat pipe was normal to the cooling airflow. A photograph of the device being tested is shown in Figure 10.

The external temperatures of the evaporator and condenser sections were measured as well as internal evaporator and condenser temperatures and vapor pressure. Vapor pressure measurements were converted into equivalent temperatures by employing a thermal properties handbook (Reference 19). All measurements were conducted approximately 1 hour after start-up (power on) for applied powers of 5, 12, and 20 watts. The heat pipe was operated in the vertical and near horizontal (evaporator elevated 1 inch) positions. In the vertical mode, gravity forces aided condensate return to the evaporator; in the near-horizontal position condensate return was promoted by capillary pumping.

b. Radiation Cooled Tests

Radiation cooled tests were conducted by placing the device inside a 12-inch-diameter x 19-inch-long cylindrical liquid nitrogen cryowall with copper end plates. Both the condenser and the internal surfaces of the cryowall were painted with flat-black enamel ($\epsilon_o \simeq .95$). The cryowall was installed in a

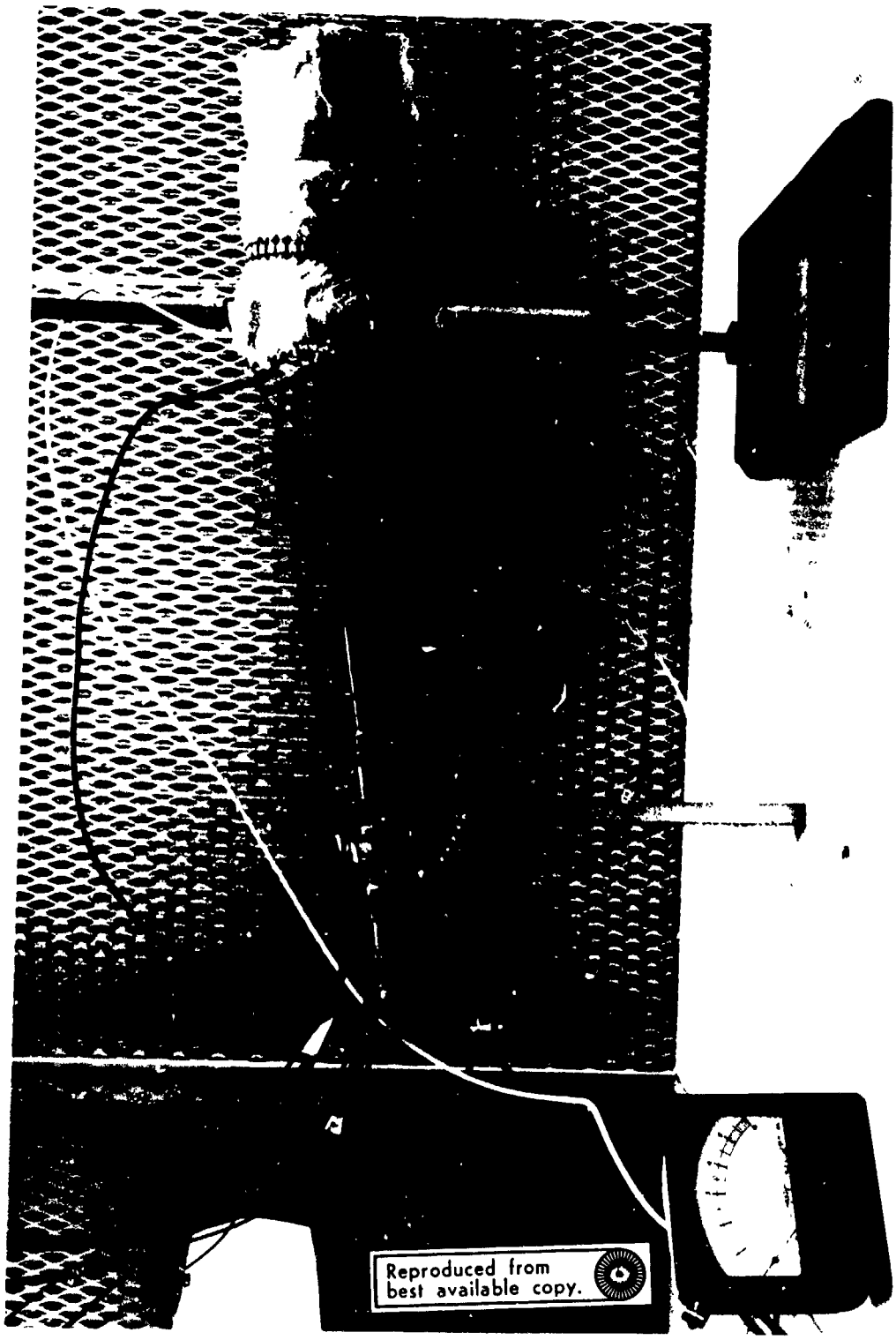

Figure 10. Planar Heat Pipe on Laboratory Clean Bench Station

3-foot-diameter and 3-foot-long vacuum chamber, and the entire system was evacuated to 10^{-6} - 10^{-7} mm Hg. The cryowall was cooled to -50°F to simulate near-earth space sink temperature and to -320°F to simulate deep-space sink temperature. Power was applied and temperature and pressure were monitored as in the forced convection tests. Figure 11 shows the vacuum chamber test setup.

c. Copper and Aluminum Fin Tests

To compare the heat-pipe temperature profile with those of metallic thermal conductors, we constructed fins of copper and aluminum. The bar of solid hard copper having the same external dimensions (1/2" x 3-1/2" x 12") was instrumented with #24 copper-constantan thermocouples and subjected to test. To duplicate the radiative properties of the heat pipe, these metal fins were also sprayed with black enamel. The aluminum fin had been suggested as a lightweight intercell conduction strap for an advanced battery design (Reference 20).

The aluminum fin weighed 0.59 pounds (270 gm), the copper fin weighed 6.8 pounds (3130 gm), and the planar heat pipe without instrumentation, valves, and fill tubes was estimated to weigh 1.25 pounds (570 gm). The copper and aluminum fin are pictured with the planar heat pipe (left) in Figure 12. Figure 13 shows the copper fin installed in the test position inside the nitrogen cryowall; the end plate of the cryowall was removed for this photograph.

Figure 11. Vacuum Chamber Test Setup and Measurement Apparatus

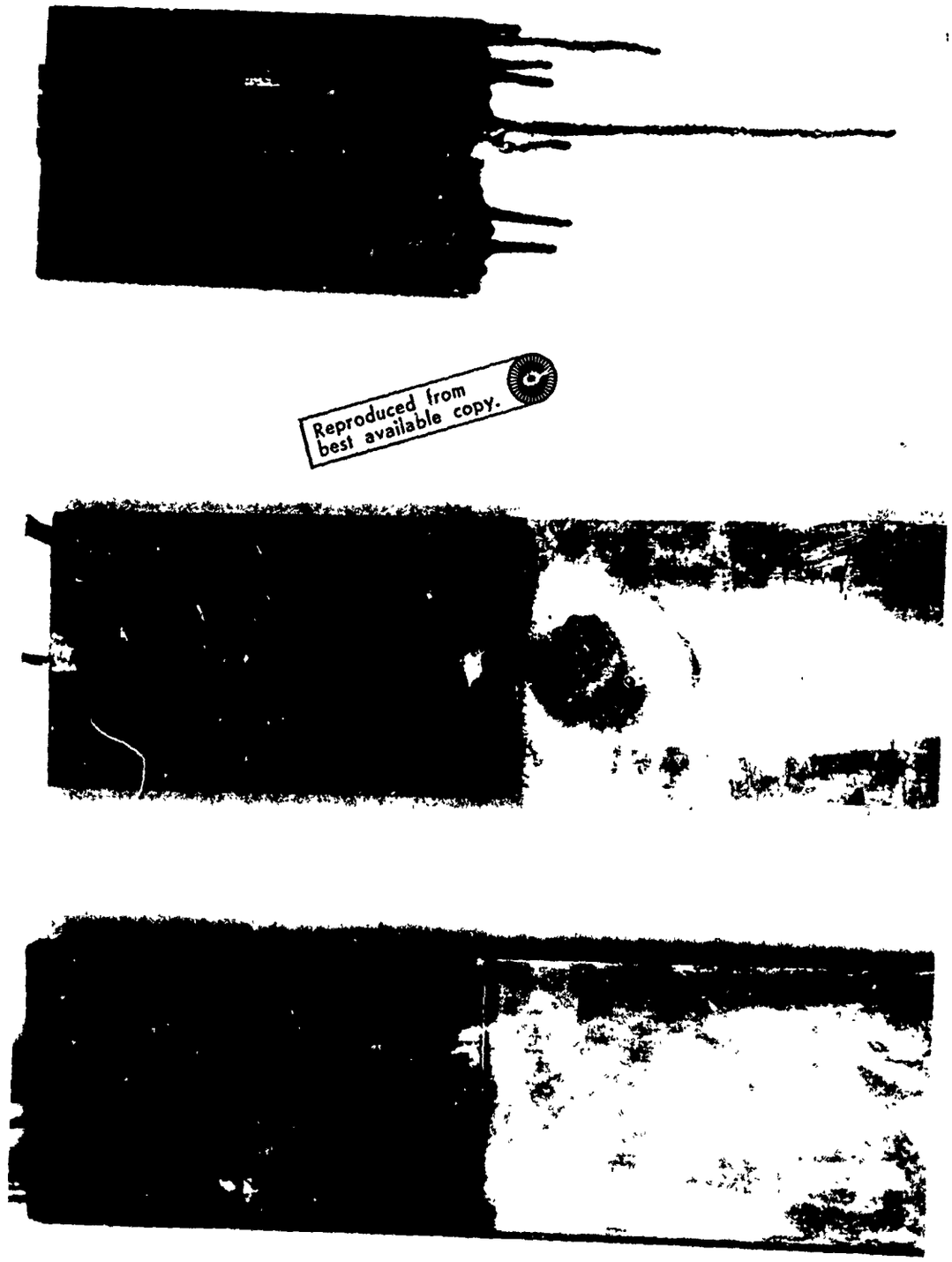

Figure 12. Copper and Aluminum Fins Shown with Planar Heat Pipe

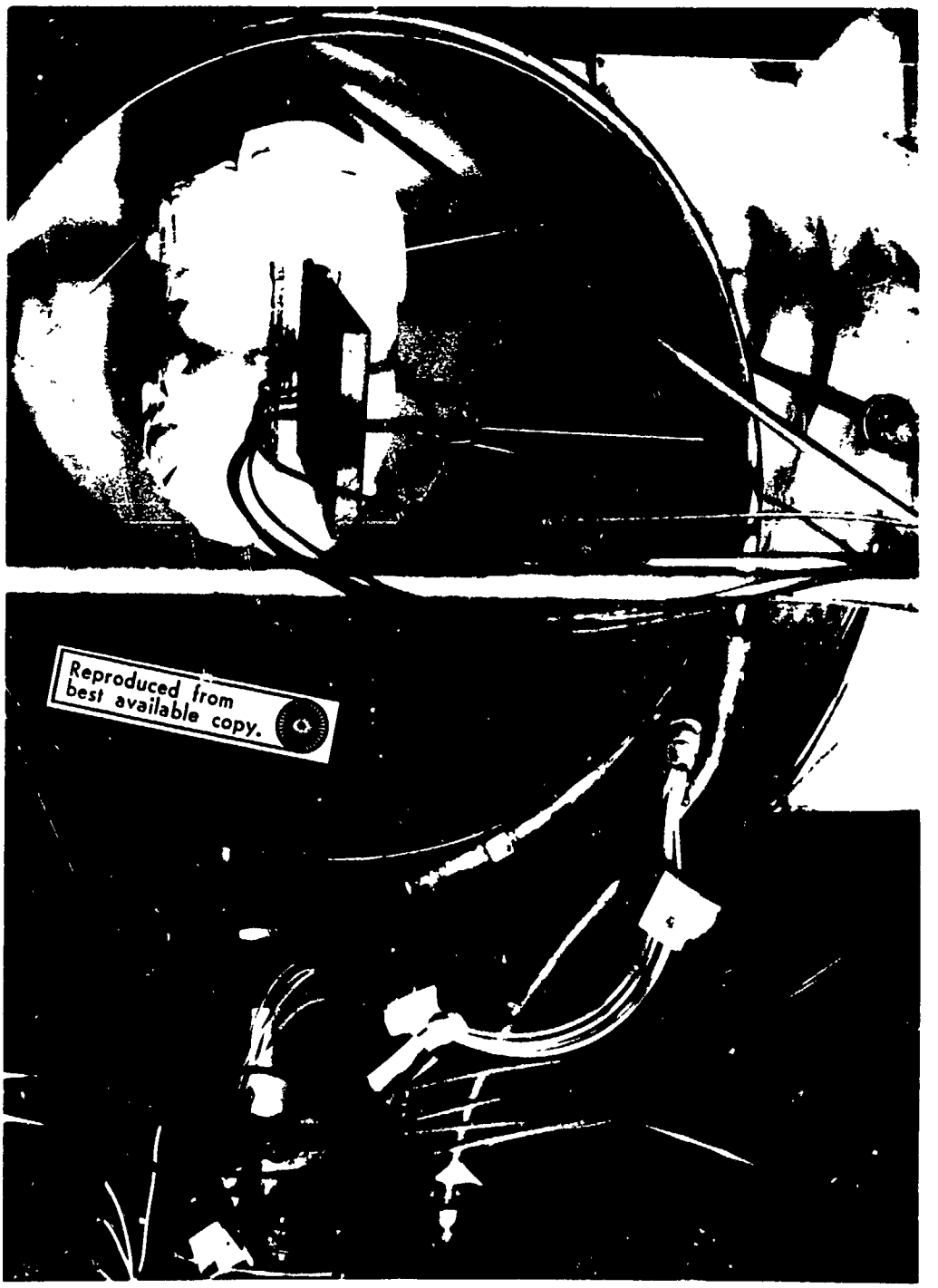

Figure 13. Copper Fin Installed in Vacuum Chamber Cryowall

SECTION IV

EXPERIMENTAL RESULTS

1. GENERAL

The planar heat pipe was tested under a variety of conditions, including applied power, amount of working fluid, and orientation with respect to gravity. For the forced convection tests, all measurements were made after one hour of operation, when the device had reached thermal equilibrium. The in vacuo test data are nonequilibrium observations.

2. FORCED CONVECTION COOLED TEST RESULTS

a. Demonstrated Heat Pipe Mode of Operation

Figure 14 presents data for the planar heat pipe in three modes of operation. Curve A represents results of 2 tests in the normal heat pipe mode, using 12 watts of applied power and 32 grams of working fluid. Curve B shows the temperature profile with no working fluid; axial heat transfer is purely by conduction. Curve C represents operation in the air-flooded mode; the heat pipe was filled with 16 grams of water, but prior to test, the fill valve was opened, allowing air to flood the pipe. The valve was then reclosed. Air flooding prevented normal heat pipe operation (see Section V). For these tests the ambient temperature was 72-74°F.

b. Temperature Profile as a Function of Applied Power

Figure 15 shows the axial temperature profile with the planar heat pipe using 24 grams of working fluid for 5, 12, and 20 watts of applied power. Ambient temperature for these runs was 74°F. Internal temperature profiles are also shown for each case, based on internal evaporator and condenser thermocouple readings. These forced convection tests were run sequentially; that is, after the 5-watt 1-hour test was run, the 12-watt 1-hour test and then the 20-watt 1-hour test were conducted without intermittent cooling.

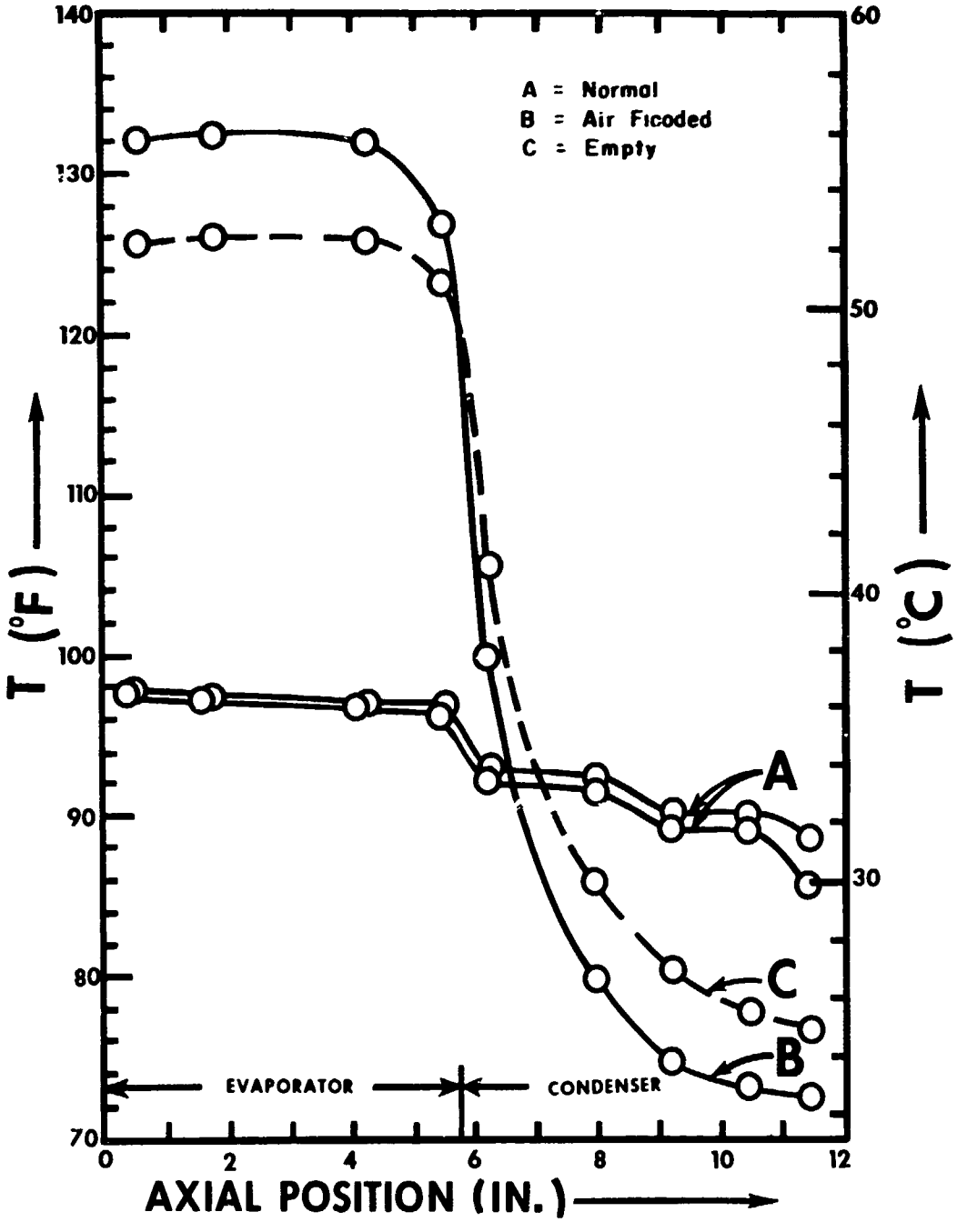

Figure 14. Results of Planar Heat Pipe Operation in Three Modes

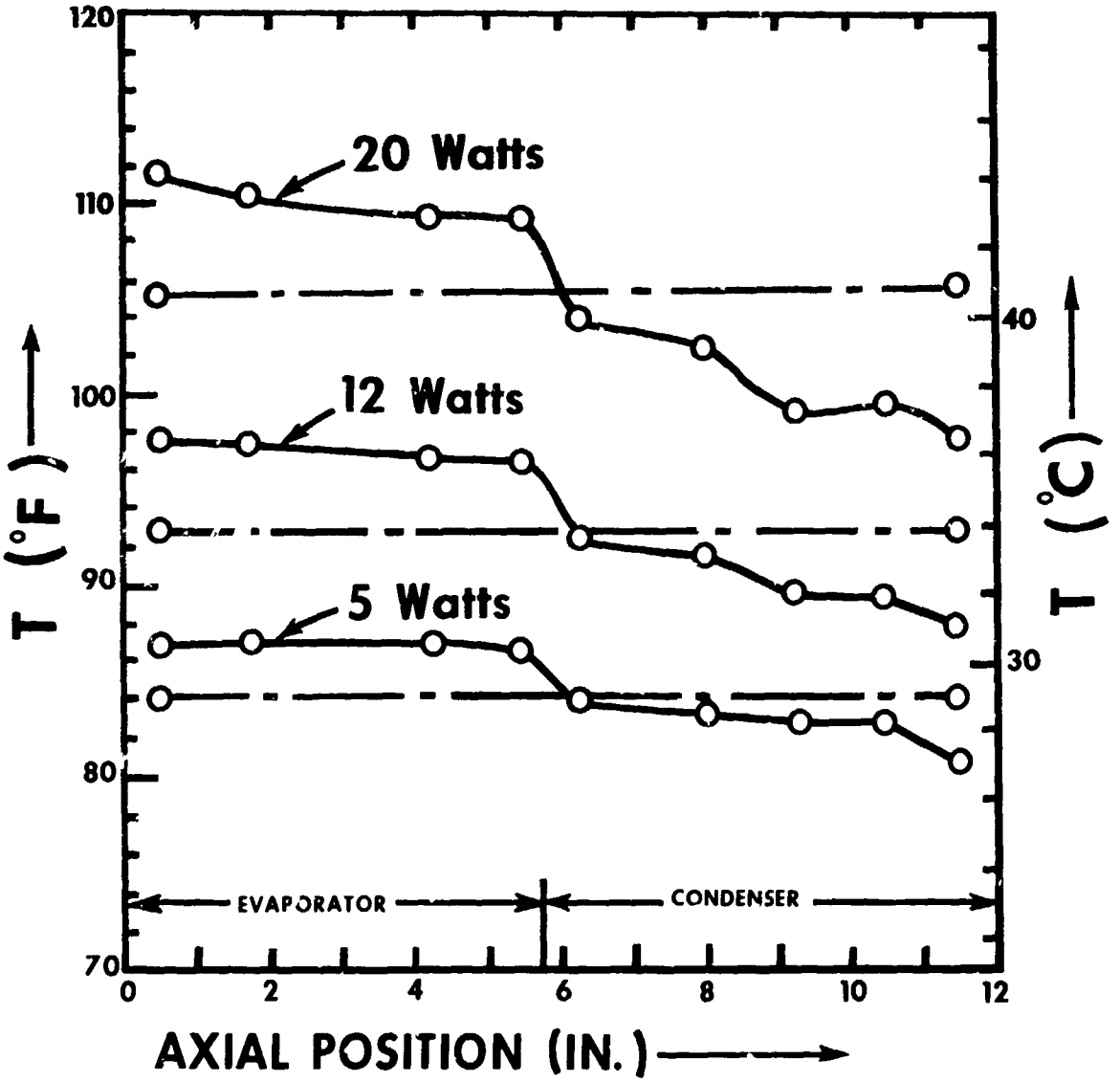

Figure 15. Planar Heat Pipe Axial Temperature Profile as a Function of Applied Power, Near Horizontal, Forced Convection Tests

c. Influence of Gravity on Temperature Profile

The heat pipe was tested both in the vertical (reflux mode) and the near-horizontal positions. In the near-horizontal position, the evaporator section was elevated 1 inch with respect to the condenser to ensure that liquid return was by capillary pumping. Figure 16 compares the temperature profile when using 32 grams of working fluid after a 1-hour near-horizontal run and a 15-minute vertical run without intermittent cooling. The ambient temperature was 71-72°F for the 20-watt tests and between 75 and 73°F for the 5 and 12 watt runs. It is evident that gravity had little influence on the performance under these conditions. The heat pipe was not capable of the same nearly isothermal performance when tested in the vertically inverted position (i.e., condenser section up) due to limited maximum wicking height of the 100-mesh capillary screen (see Table XII).

d. Variation in Amount of Working Fluid

Based on the calculations described in Appendix IV, we estimated the amount of water necessary to saturate the capillary screen to be approximately 22 grams. This calculation considers the actual thickness of two layers of stainless steel screen. The individual screen layers were not bonded, either to each other or to the shell wall, however, so the actual thickness of the wick as installed in the heat pipe is not known exactly. Visual inspection indicated that some areas of the screen layers had nested in each other, while other areas had small interlayer gaps and undulations. Based on this uncertainty, we decided to test the device with different amounts of working fluid, varying from 8 to 64 grams. Figure 17 and Table III present the results of these tests. It was found that neither 8 nor 12 grams of water was sufficient for stable operation at 5 watts, and 16 grams was not sufficient for 20 watts. In these cases, the evaporator "burned out"; its external temperature did not stabilize after one hour of operation. The external axial temperature gradient, ΔT_{ax}, characteristically exceeded 10°F, indicating the wick in the evaporator was not being replenished with liquid. For burnout cases, normal operation could be reestablished by tilting the device and rewetting the capillary.

We decided that 32 grams of fluid would be more than adequate to prevent burnout in the power range of 5-20 watts. If the device were operated at lower powers, perhaps a smaller amount of fluid could be used to minimize the thickness

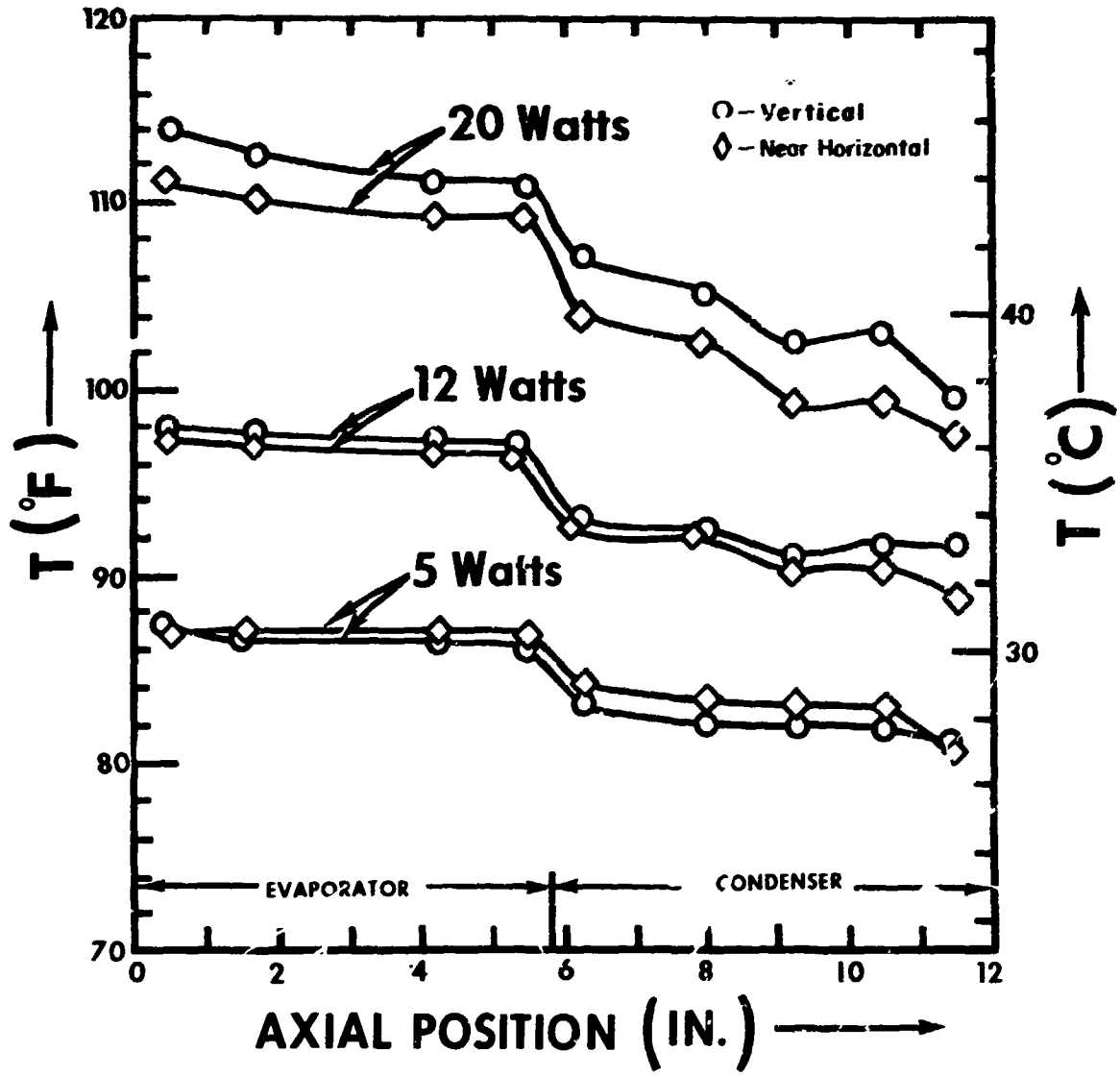

Figure 16. The Influence of Gravity on Planar Heat Pipe Axial Temperature Profile (see Text for Test Procedure)

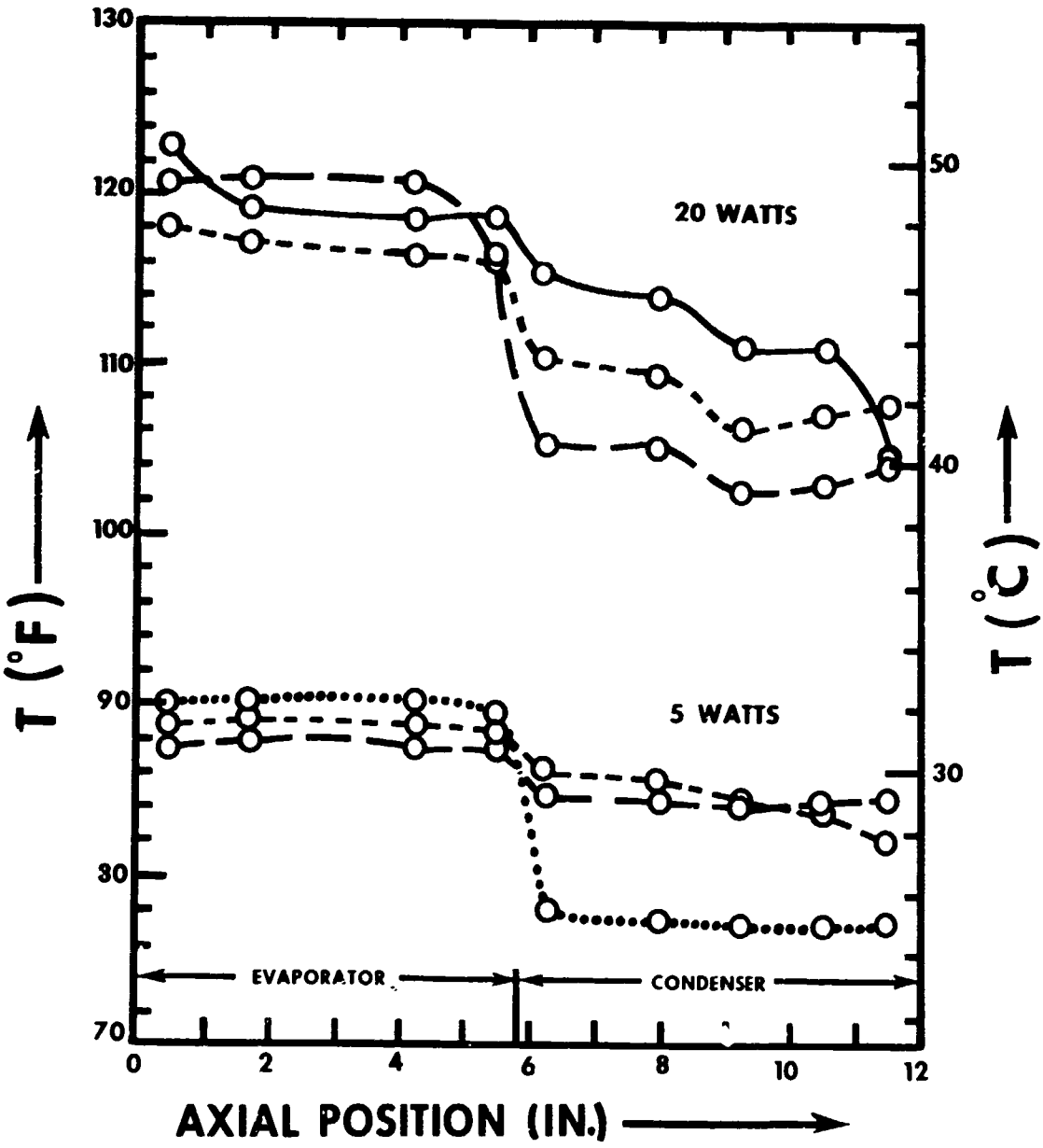

Figure 17. Effect of the Amount of Working Fluid on Planar Heat Pipe Performance—Forced Convection One Hour Test, Near Horizontal Position

TABLE III

AXIAL AND RADIAL TEMPERATURE GRADIENTS FOR VARIOUS AMOUNTS OF WORKING FLUID AND APPLIED POWER, FORCED CONVECTION COOLING, NEAR HORIZONTAL POSITION*

Power, w	Mass H_2O, gm	T_o	ΔTer	ΔT_{cr}	ΔT_{ax}	Comment
5	8	75.5	6.1	-6.7	12.7	Burnout
5	12	80.0	11.2	-2.6	13.9	Burnout
5	16	73.5	3.5	-0.1	3.5	Fill 1
5	16	79.7	2.5	-0.7	3.2	Fill 2
5	24	73.9	3.0	-1.0	4.0	Fill 1, Run 1
5	24	77.0	2.3	-0.8	3.0	Fill 1, Run 2
5	32	73.0	2.9	-1.3	4.2	Fill 1, Run 1
5	32	76.0	2.9	-1.5	4.3	Fill 1, Run 2
5	64	72.0	3.1	-2.1	4.6	
12	16	72.2	4.2	-1.9	6.0	Fill 1, Run 1
12	16	79.0	4.2	-1.4	5.6	Fill 1, Run 2
12	16	74.5	3.2	-1.6	5.6	Fill 2, Run 1
12	16	74.5	3.3	-2.0	5.2	Fill 2, Run 2
12	24	73.8	3.6	-2.3	5.8	
12	32	74.8	3.4	-3.5	5.9	
12	32	72.0	3.9	-3.3	7.2	
12	64	78.5	2.6	-3.7	6.3	
20	16	73	16.0	-3.6	19.6	Burnout
20	24	73.7	4.7	-4.9	9.6	
20	32	79.0	4.8	-4.1	8.9	
20	32	71.2	4.9	-5.5	10.0	
20	64	82.0	3.4	-5.4	8.8	
20	64	77.6	3.4	-4.9	8.3	

*Legend - Mass H_2O - Amount of working fluid
T_o - Ambient Temperature
ΔT_{er} - Evaporator radial temperature gradient
ΔT_{cr} - Condenser radial temperature gradient
ΔT_{ax} - Mean axial external temperature gradient

of the liquid layer and thus the radial evaporator and condenser temperature gradients.

3. RADIATION COOLED TESTS

The planar heat pipe was subjected to vacuum chamber testing, using a liquid nitrogen cryowall as a radiation heat sink. The tests were initiated with the cryowall and heat pipe at ambient temperature, typically 75 to 80°F. Liquid nitrogen was supplied to the cryowall and electrical power to the heaters simultaneously. The cryowall reached equilibrium at -50°F after 15 to 20 minutes of cooling and at -320°F after 30-35 minutes. For radiation-cooled tests, the heat pipe was in the near-horizontal position.

The heat pipe would not operate properly at -320°F sink temperature. Figure 18 shows the time-varying temperature profiles for the device for 5 and 20 watts applied power. The test was initiated with 5 watts applied power, and the temperature of the heat pipe decreased steadily with large axial gradients. After two hours the internal evaporator thermocouple indicated +21°F, but the evaporator was frozen. In an attempt to thaw the heat pipe, the power was increased to 20 watts. This succeeded in thawing the evaporator, but the condenser temperature continued to drop. After 60 minutes with 20 watts applied, the internal evaporator and condenser temperatures were +69°F and -39°F, respectively. The vapor was flowing to the condenser and freezing, precluding the liquid return to the evaporator via capillary pumping. The test was terminated.

Radiation cooled tests for -50°F sink temperature were more positive. As shown in Figure 19, the heat pipe cooled continuously, approaching equilibrium after two hours with 5 watts applied. At 12 and 20 watts, it cooled initially, but then the temperature began to increase, and after 90 minutes the device had not reached equilibrium. The tests were terminated. The small anomaly of the thermocouple at the 9-inch position suggests a small mechanical printing error may have existed in the Brown recorder print wheel.

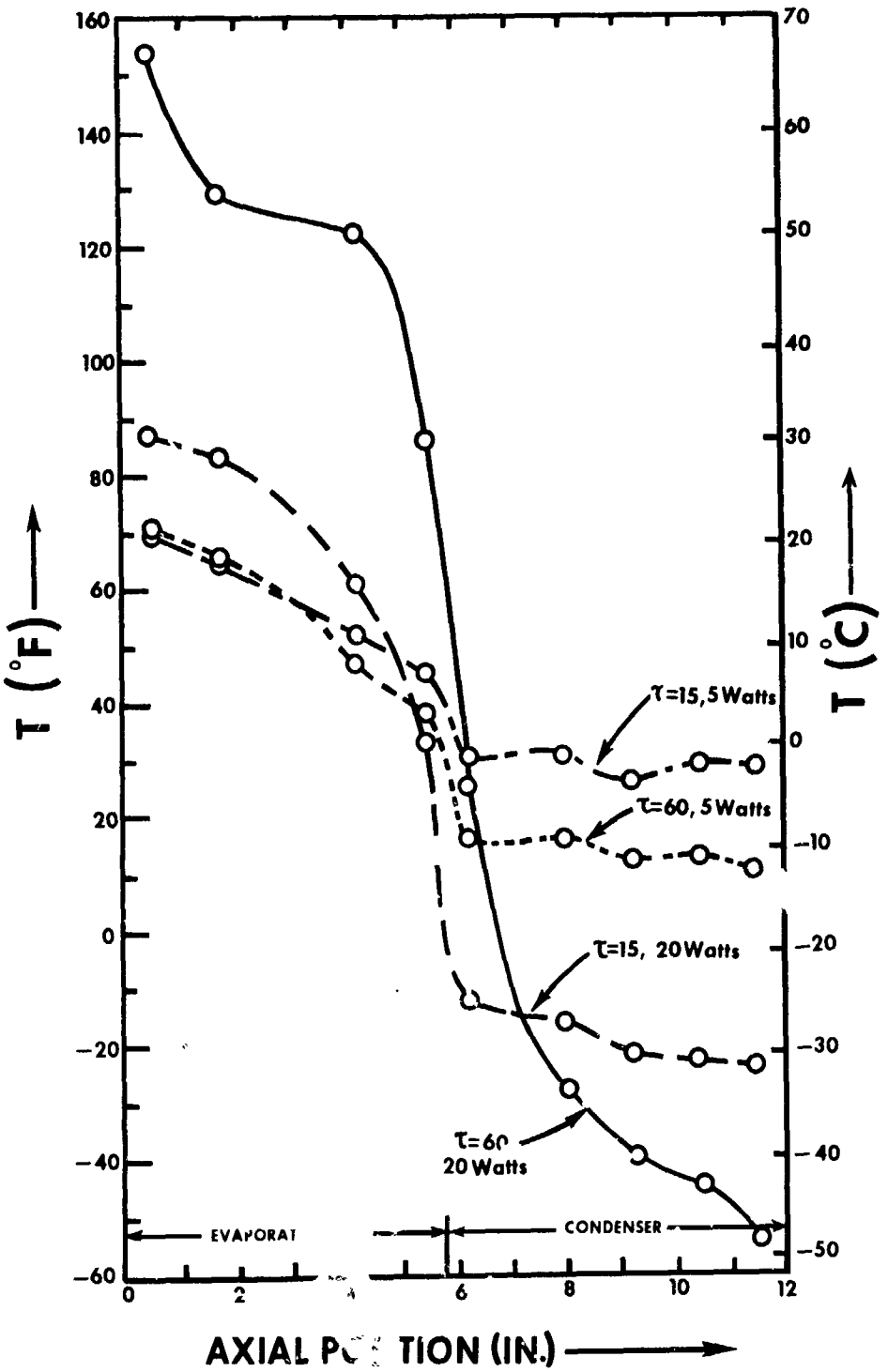

Figure 18. Transient Thermal Response for Planar Heat Pipe, -320°F Radiation Heat Sink Test

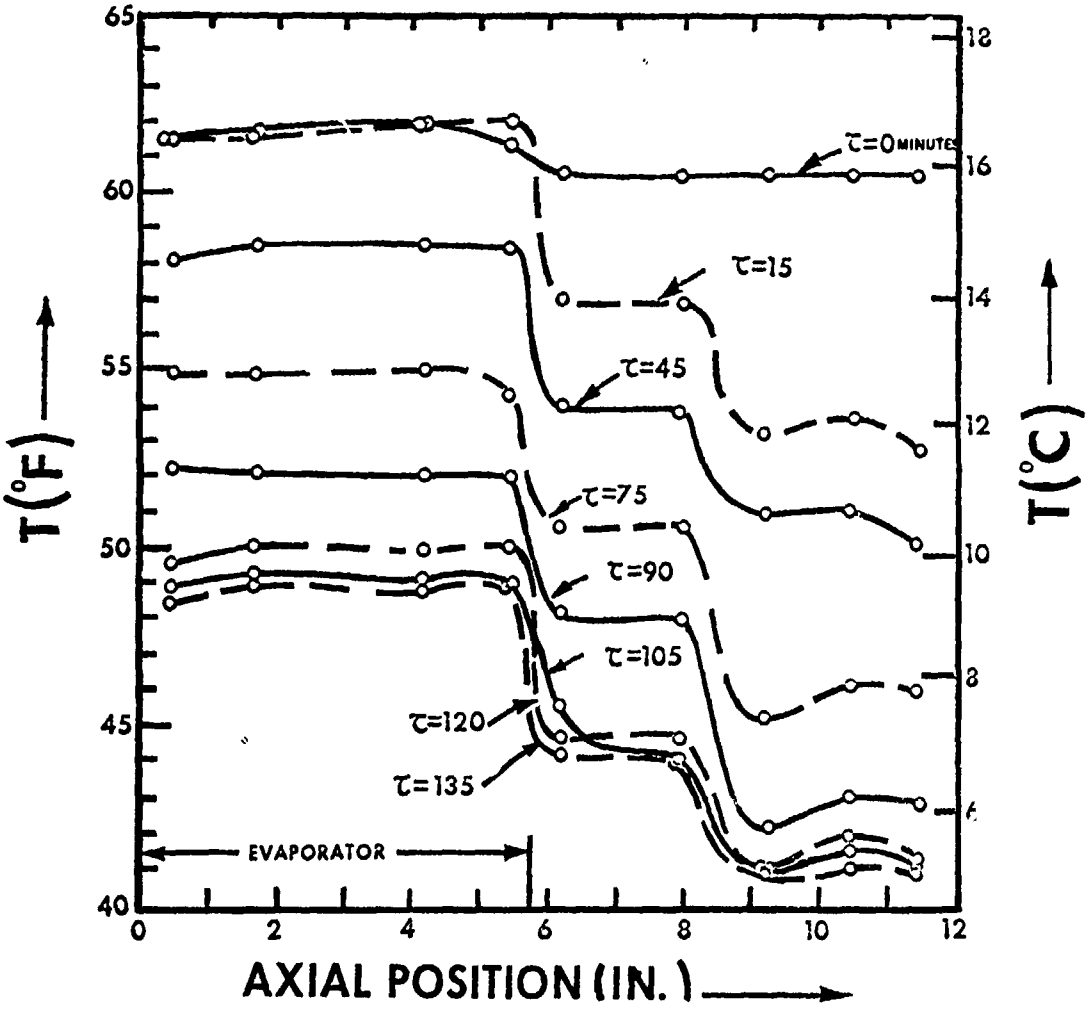

Figure 19. Transient Thermal Response for Planar Heat Pipe, -50°F Radiation Heat Sink Test

Table IV summarizes the internal temperature - time response of the heat pipe for both the -320°F and -50°F heat sink tests described above. It was concluded that the area of the condenser radiator of the heat pipe was excessive for the -320°F heat sink conditions, so the net radiated power exceeded the applied power, and the working fluid froze. In the -50°F heat sink condition, the area of the condenser radiator was not sufficient to allow operation at 12 and 20 watts applied power in the operational temperature range (32-120°F) of interest. A frozen start-up of the heat pipe was not attempted due to the difficulties in establishing thermal equilibrium.

To investigate equilibrium temperature profiles with radiative cooling, the device was to be run overnight for at least 12 hours. The cryowall temperature was manually controlled by a LN_2 metering valve, however, so 12-hour test was conducted with the cryowall uncooled. The tests were initiated with the cryowall and heat pipe at room temperature (75°F). The temperature profile of the heat pipe after a 12-hour run is shown in Figure 20.

4. COMPARATIVE TEMPERATURE PROFILES FOR SOLID COPPER AND ALUMINUM FINS

Figures 21, 22, and 23 compare the measured temperature profiles of the copper and aluminum fins to those of the heat pipe for 1-hour test runs at 5, 12, and 20 watts with forced convection cooling. The tests were run sequentially with no intermittent cooling of either the fin or the heat pipe. Ambient temperature conditions between these runs varied by only 1 to 3°F.

Figure 24 compares the nonequilibrium temperature profiles of the copper fin and the heat pipe for -50°F radiation heat sink conditions. The thermal response of the heat pipe is much more rapid than that of the copper fin, but after 90 minutes the temperature profiles are nearly identical.

The temperature profile of the copper fin and heat pipe for the 12-hour, 12-watt radiation test are shown in Figure 25. The temperature profiles are remarkably similar for this equilibrium condition. The ambient temperature for the heat pipe test was 75°F, approximately three degrees higher than that for the copper fin test. Because of this temperature difference, no valid

TABLE IV

INTERNAL TEMPERATURE MEASUREMENTS FOR PLANAR HEAT PIPE DURING RADIATION COOLED TESTS, 32 GMS H_2O, NEAR HORIZONTAL POSITION

T_o (°F)	Power (w)	Time (min)	T_{ie}* (°F)	T_{ic}** (°F)	T_p*** (°F)
-320	5	0	72.0	72.0	72.0
-320	5	75	35.7	34.4	40.0
-320	5	120	21.0	18.5	-
-320	20	0	21.0	18.5	-
-320	20	30	29	-17.0	-
-320	20	60	69	-39.0	-
-50	5	0	72.5	72.5	72.5
-50	5	30	58.4	57.5	58.5
-50	5	60	54.2	53.2	54.0
-50	5	90	49.7	48.6	47.2
-50	5	120	47.0	46.2	47.0
-50	5	150	45.8	45.0	47.0
-50	5	165	45.0	43.9	47.0
-50	12	0	45.0	43.9	47.0
-50	12	30	51.0	50.4	52.2
-50	12	70	61.0	60.5	60.5
-50	12	90	68.4	68.9	67.5
-50	20	0	68.4	68.9	67.5
-50	20	30	94.8	95.1	-
-50	20	60	110.2	111	-
-50	20	90	119.0	119.5	114.5

* T_{ie} - Evaporator internal thermocouple measurement
** T_{ic} - Condenser internal thermocouple measurement
*** T_p - Temperature correlation of vapor pressure measurement

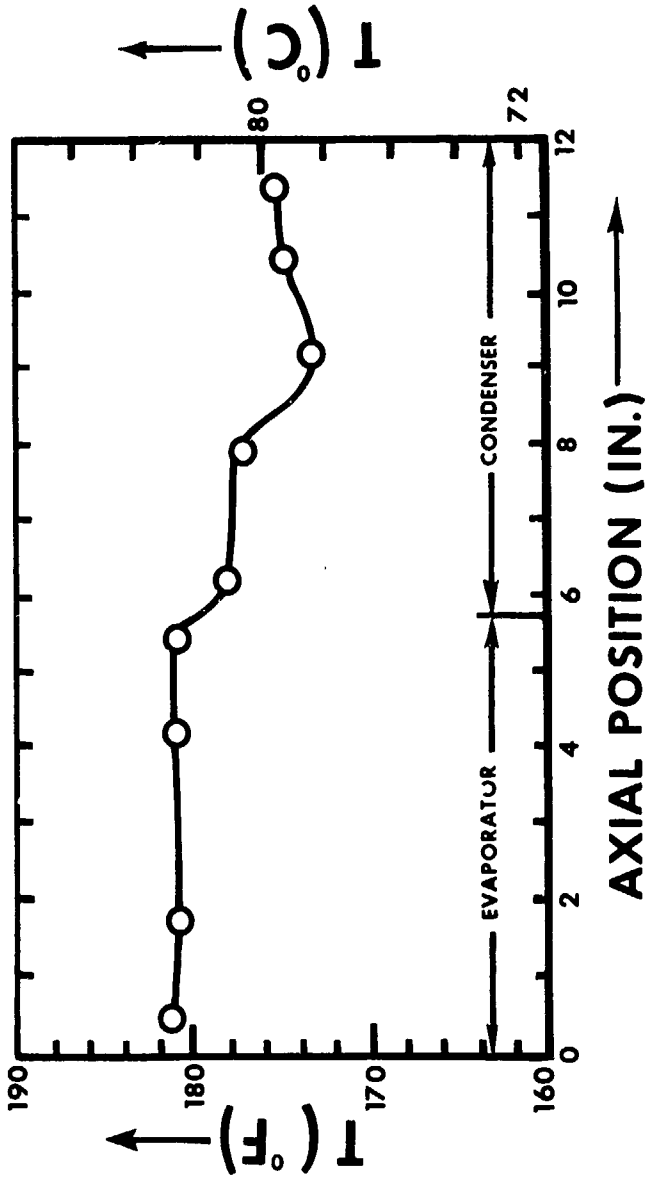

Figure 20. Equilibrium Axial Temperature Profile for Planar Heat Pipe, 12-Hour Radiation Cooled Test (Cryowall Off)

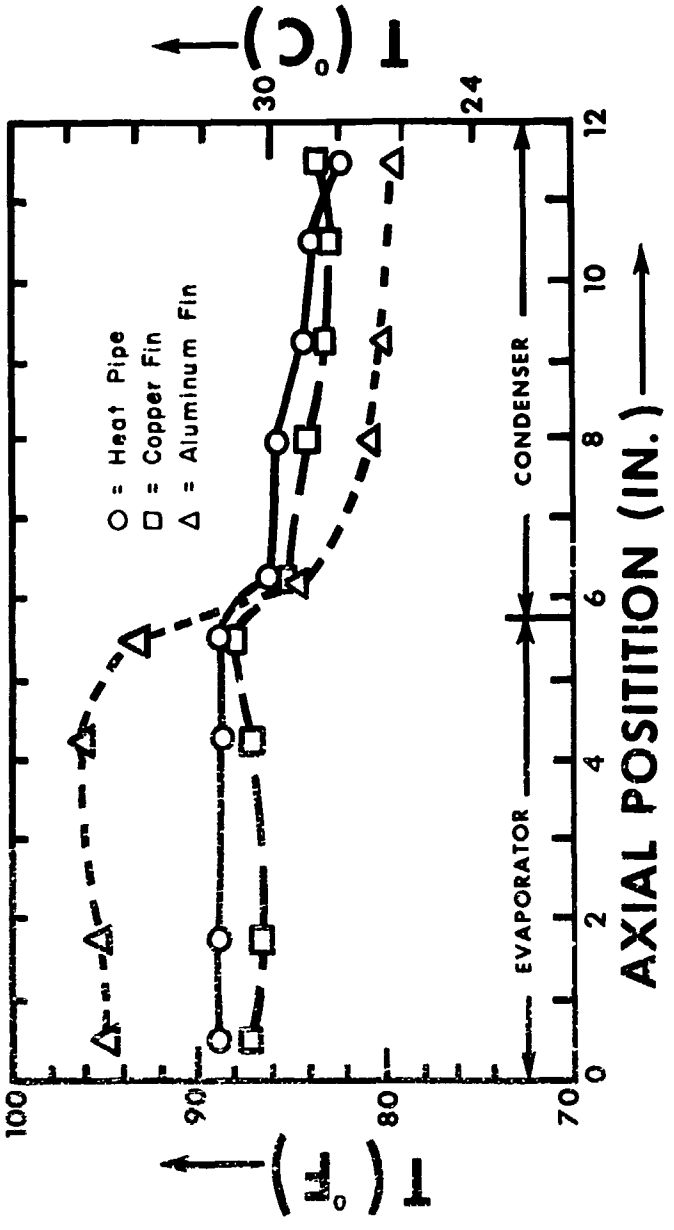

Figure 21. Axial Temperature Profile of the Planar Heat Pipe Compared to Copper and Aluminum Fins, 5 Watts, One Hour Forced Convection Cooled Tests, No Preheat

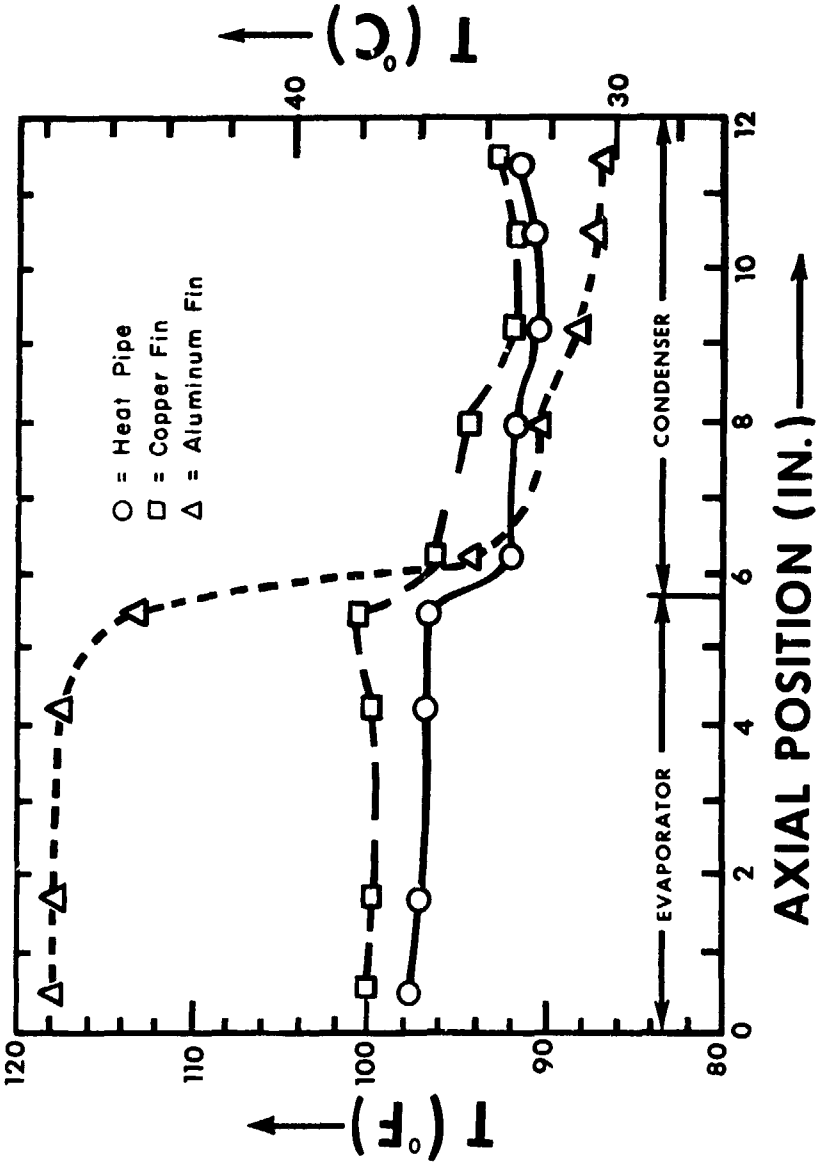

Figure 22. Axial Temperature Profile of the Planar Heat Pipe Compared to Copper and Aluminum Fins, 12 Watts, One Hour Forced Convection Cooled Tests, 5 Watt Hours Preheat

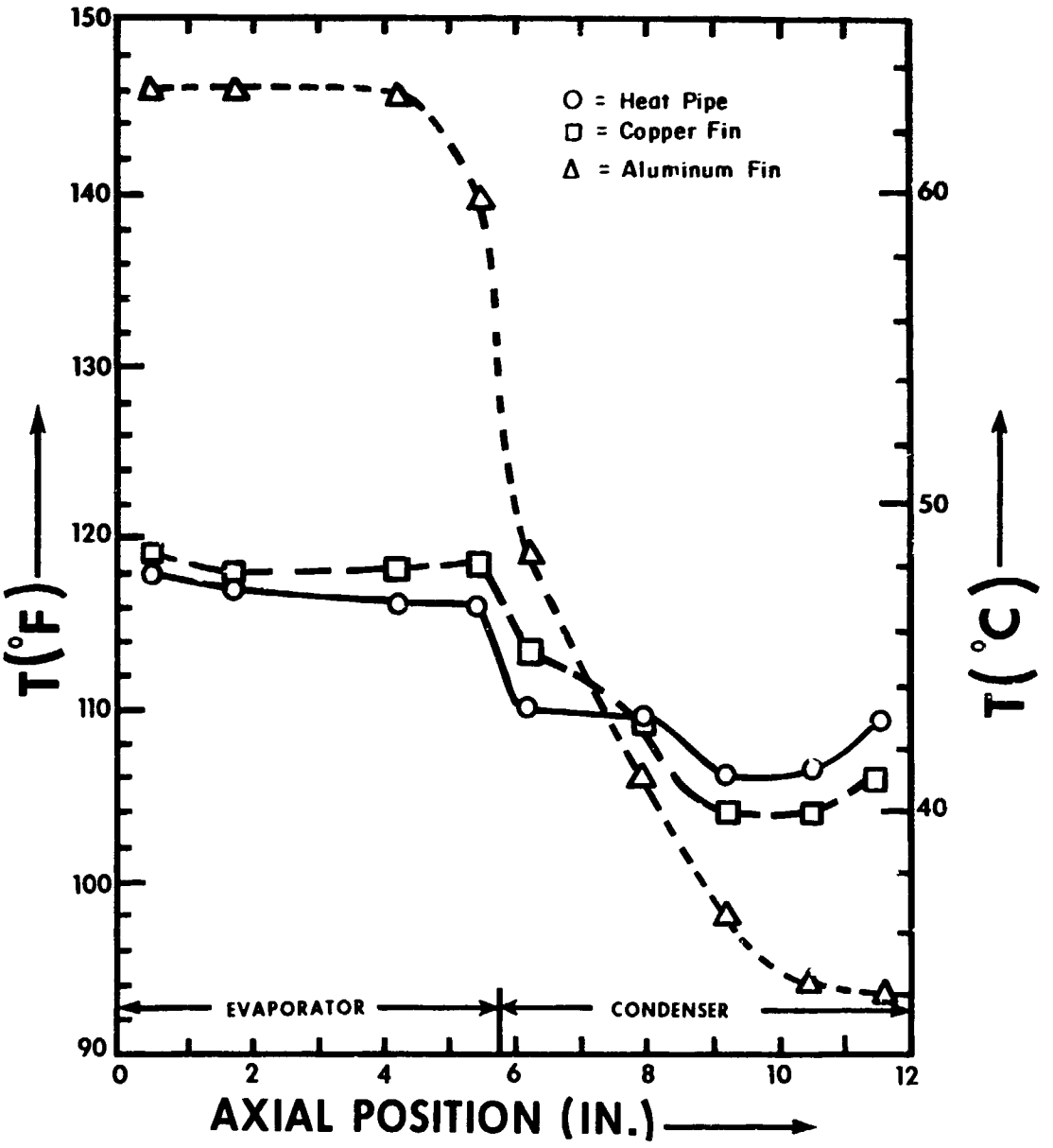

Figure 23. Axial Temperature Profile of the Planar Heat Pipe Compared to Copper and Aluminum Fins, 20 Watts, One Hour Forced Convection Cooled Tests, 17 Watt Hours Preheat

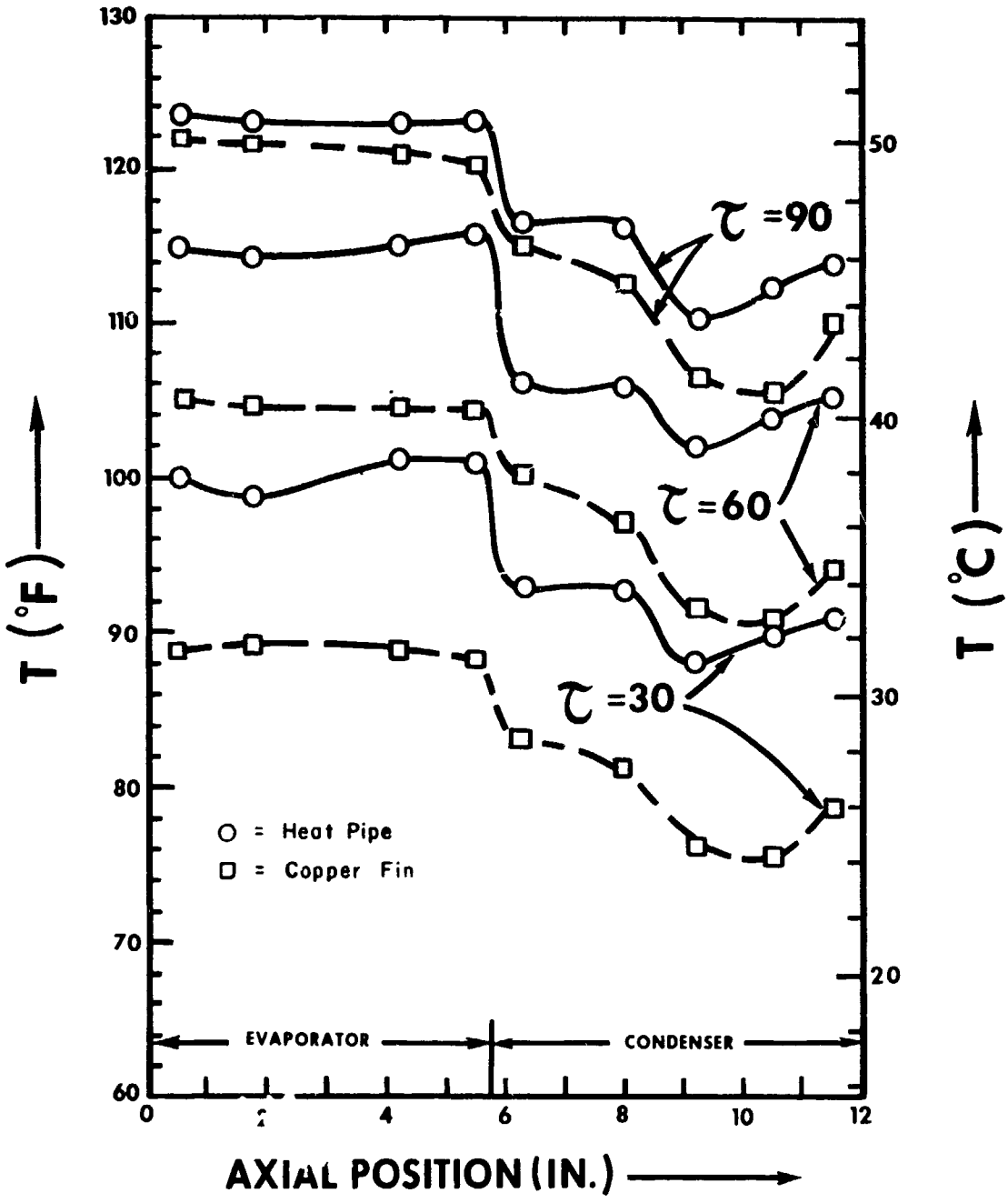

Figure 24. Transient Thermal Response for Planar Heat Pipe and Copper Fin for 20 Watt, -50°F Radiation Heat Sink Test

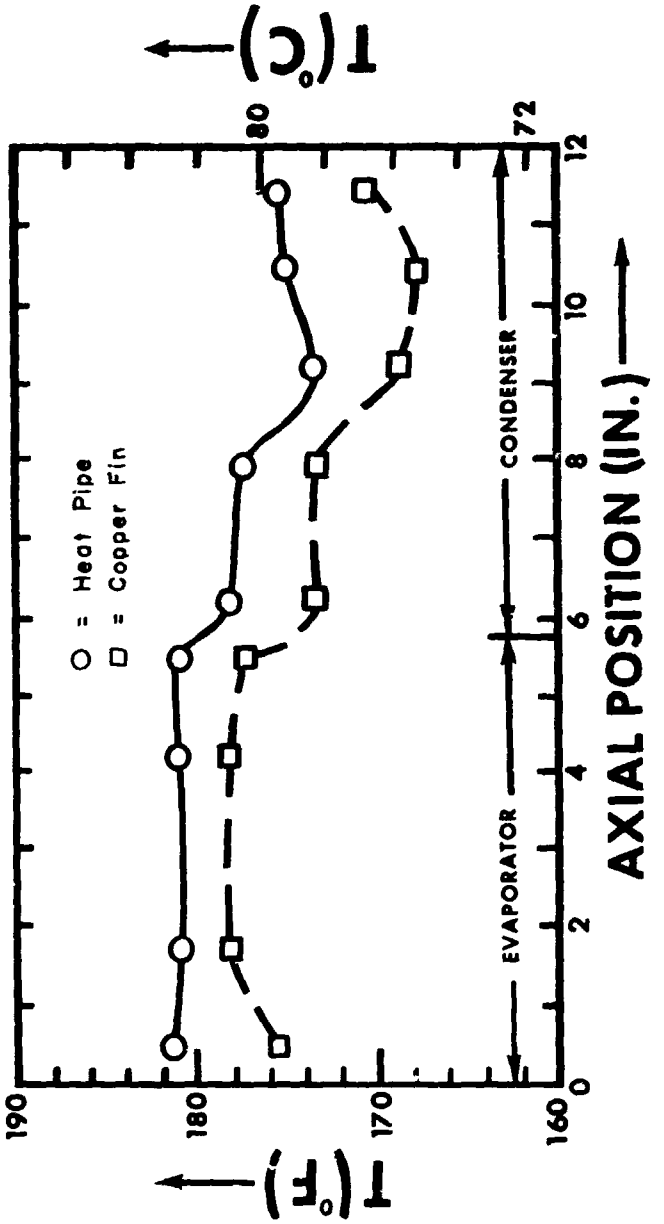

Figure 25. Heat Pipe and Copper Fin Temperature Profiles for 12 Hour Radiation Cooled Test (Cryowall Off)

comparison of the radiative heat transport characteristics can be made. No further radiation cooled tests with the cryowall off were made because this condition is not representative of a spacecraft application.

SECTION V

ANALYSIS OF TEST RESULTS

1. ESTIMATE OF EXPERIMENTAL ERROR

a. Thermocouple Measurements

As described in Section III, calibrating the thermocouple/Brown Recorder printout system against the Dymex quartz thermometers showed a mean error of 0.56°F over the range of 32 to 159°F. The Brown Recorder thermocouple printout could be read to approximately 0.2°F accuracy. Thus, the accuracy of the thermocouple recordings is ±0.56°F.

b. Pressure Measurements

The calibration accuracy of the CEC pressure transducer was 0.05% full-scale or ±0.001 psia. The printout of the Brown millivolt printer used to monitor and record pressure transducer outputs could be read to only two decimal places or ±0.01 psia. In the pressure and temperature range of these experiments, this limited the accuracy of the temperature measurement as correlated from the vapor pressure to approximately ±0.5°F.

c. Power Measurements

The Weston Ammeter and Voltmeter scale graduations could be read to 0.01 amps and 0.01 volts, respectively. These devices were calibrated to 2.0% and 0.5%, respectively. The power settings are shown in Table V. Since #12 copper wire was used as the power lead and voltage was sensed at the heater connect, power losses in the leads were negligible.

d. Evaporator Insulation Losses

The evaporator and heater plates were wrapped on four sides and on the bottom with 1-1/2 inches of Carborundum Fiberfrax insulation; the manufacturer specifies the thermal conductivity of this material to be 0.06 BTU/hr ft °F at 400°F. Neglecting heat losses out of the uninsulated top faces of the heater plates and assuming the thermal conductivity quoted by themanufacturer at 400°F to be applicable to the temperature range of these experiments, the maximum

TABLE V

POWER SETTINGS AND MEASUREMENT ERROR

Nominal Power	Ammeter Setting	Volts	Actual Power	%Error
5 Watts	1.33a	3.75v	4.9875 Watts	0.25%
12 Watts	2.0 a	6.0 v	12.00 Watts	0%
20 Watts	2.61a	7.65v	19.967 Watts	0.165%

power loss due to conduction losses through the insulation are computed as 0.4, 0.8, and 1.6 watts for applied power of 5, 12, and 20 watts. This estimate is based on an approximate temperature gradient through the insulation, nominally 10°F, 20°F, and 40°F for 5, 12, and 20 watts applied power, respectively.

The heat loss through the uninsulated heater ends can also be estimated, using an empirical value for the film heat transfer coefficient of a vertical flat plate (heater ends) to air, given by McAdams as 0.6 BTU/hr ft^2 °F (Reference 21). For the total area of the heater ends (3 sq in), assuming a ΔT of 20°F, the heat loss from the uninsulated heater end to the air is approximately 0.12 watts.

Physical reasoning can be used to substantiate this value. Copper and stainless steel provide a relatively low thermal resistivity (reciprocal of thermal conductivity) heat path, while that of air is several orders of magnitude greater.

e. Overall Experimental Error

The temperature measurements reported herein are estimated to be accurate to at least ±1°F, and the power measurements to at least 1%. Maximum thermal loss in the evaporator was approximately 10% of the applied power.

2. CORRELATION OF INTERNAL TEMPERATURE MEASUREMENTS

Tables VI and VII present the internal thermocouple measurements for the forced convection tests. In both the near horizontal position (Table VI) and the vertical position (Table VII), the internal axial temperature gradient (ΔT_i) is small, typically less than 0.5°F. A pecularity of these data is the negative value for the evaporator-to-condenser internal temperature gradient, ΔT_i. This might be attributed to experimental error and/or poor thermocouple contact with the evaporator internal surface.

Correlation of the condenser thermocouple temperature (T_{ic}) and pressure transducer correlated temperature (T_p) measurements is shown for the forced convection tests for the near horizontal and the vertical positions in Table VIII and IX, respectively. In the near-horizontal position, the agreement was good. In general, the thermocouple temperature was slightly lower than the pressure transducer table correlated temperature.

In the vertical position, agreement between the two measurements was not good; significant temperature gradients were noted, corresponding to a 0.1 - 0.2 psia pressure drop from the condenser to the pressure transducer, which was located approximately 3 inches away from the condenser section on the 3/8" pressure tap pipe. Calculations of change in hydrostatic pressure differential due to the difference in elevation showed it to be negligible. The only apparent source of the discrepancy was a small amount of incondensible gas being trapped in the pressure tap pipe; in the horizontal position this would not interfere with the volume of condensible vapor flowing into the pressure tap pipe and transducer. In the vertical position, however, a slug of incondensible gas with a density less than that of water vapor would migrate to the uppermost part of the heat pipe (i.e., the pressure tap tube) where it would prevent the condensible gas from reaching the pressure transducer, and thus cause a temperature gradient.

A diffusion barrier of incondensible gas is the principle of operation of the "variable conductance" heat pipe. In effect, the incondensible gas allows the heat pipe to operate at nearly constant temperature for a range of input powers by regulating the condenser heat rejection area. As the vapor pressure

TABLE VI

INTERNAL TEMPERATURE MEASUREMENTS FOR PLANAR HEAT PIPE IN NEAR HORIZONTAL POSITION, FORCED CONVECTION COOLED

Power (w)	Mass H_2O, (gm)	T_{ie} (°F)	T_{ic} (°F)	ΔT_i (°F)	Comment
20	64	117.0	116.0	+1.0	
20	32	111.9	112.0	-0.1	Fill #1
20	32	105.3	105.8	-0.3	Fill #2
20	24	107.0	107.2	-0.2	
20	16	101.0	101.0	-0.0	Burnout, Fill #1
20	16	106.5	106.8	-0.3	Burnout, Fill #2
12	64	97.8	98.0	-0.2	
12	32	93.4	93.8	-0.4	Fill #1
12	32	93.0	93.2	-0.2	Fill #2
12	24	92.1	92.2	-0.1	
12	16	92.6	93.0	-0.4	Fill #1
12	16	87.8	87.9	-0.1	Fill #2
5	64	82.4	81.8	+0.6	
5	32	84.1	84.1	0.0	Fill #1
5	32	85.8	85.8	0.0	Fill #2
5	24	81.3	81.3	0.0	
5	16	81.0	81.2	-0.2	Fill #1
5	16	84.8	84.9	-0.1	Fill #2
5	8	83.8	83.9	-0.1	Burnout

TABLE VII

INTERNAL TEMPERATURE MEASUREMENTS FOR PLANAR HEAT PIPE
IN VERTICAL POSITION, FORCED CONVECTION COOLED

Power (w)	Mass H_2O (gm)	T_{ie} (°F)	T_{ic} (°F)	ΔT_i (°F)	Comment
20	64	118.0	116.0	+2.0	
20	64	107.8	107.0	+0.8	Cold Start
20	64	113.5	112.1	+1.4	
20	32	112.4	113.0	-0.6	
20	32	93.3	93.8	-0.5	
20	24	106.8	107.2	-0.4	
20	16	101.5	101.9	-0.4	
20	16	108.0	108.2	-0.2	
12	64	108	108.2	-0.2	
12	32	93.3	93.8	-0.5	
12	24	92.3	92.5	-0.3	
12	16	93.4	93.8	-0.4	
5	64				Not run
5	32	83.2	83.2	0.0	
5	24	81.3	81.4	-0.1	
5	16	81.0	81.2	-0.2	
5	8	83.0	83.0	-0.0	

TABLE VIII

COMPARISON OF CONDENSER THERMOCOUPLE AND PRESSURE TRANSDUCER MEASUREMENTS, NEAR HORIZONTAL POSITION, FORCED CONVECTION COOLED

Power (w)	Mass H_2O, (gm)	T_{ic} (°F)	T_p (°F)	p (psia)	$T_{ic} - T_p$	Comment
20	64	116.0	117	1.55	-1.0	
20	32	112.0	113	1.39	-1.0	Fill #1
20	32	105.8	106	1.16	-0 2	Fill #2
20	24	107.2	107.3	1.18	-0..	
20	16	101.0	102	1.00	-1.0	Fill #1
20	16	106.8	107.3	1.18	-0.5	Fill #2
12	64	98.0	94.6	.805	+3.4	
12	32	93.8	95	.81	-1.2	Fill #1
12	32	93.2	94.4	.80	-1.2	Fill #2
12	24	92.2	91.5	.73	+0.70	
12	16	87.9	87.5	.64	+0.40	Fill #1
12	16	98.0	97.8	.76	+0.20	
5	64	81.8	83.2	.56	-1.4	
5	32	84.1	86.5	.62	-1.4	Fill #1
5	32	85.8	87.5	.65	-1.7	Fill #2
5	24	81.3	82.4	.55	-1.1	
5	16	80.6	80.8	.52	-0.2	Fill #1
5	16	84.9	85.5	.60	-0.6	Fill #2
5	8	83.9	83.4	.57	+0.5	

TABLE IX

COMPARISON OF CONDENSER THERMOCOUPLE AND PRESSURE TRANSDUCER MEASUREMENTS, VERTICAL POSITION, FORCED CONVECTION COOLED

Power (w)	Mass H_2O (gm)	T_{ic} (°F)	T_p	P_p (psia)	$T_{ic} - T_p$	Comment
20	64	116.0	112.0	1.35	+4	Fill #1
20	64	112.1	106.0	1.10	+6.1	Fill #2
20	64	107.0	103.0	1.04	+4.0	Fill #2, 2.5 Hr.
20	32	113.0	107.8	1.19	+5.2	Fill #1
20	32	108.0	102.0	1.00	+6.0	Fill #2
20	24	107.2	104.0	1.07	+3.2	
12	64	100.0	89.5	.69	+10.5	Fill #1
12	32	93.8	91.0	.72	+2.8	Fill #1
12	24	92.5	88.8	.67	+3.7	
12	16	93.4	90	.70	+3.4	
5	64					Not Run
5	32	107.2	104	1.07	+3.2	Fill #1
5	24	81.4	80.5	.51	+0.9	
5	16	81.2	81.6	.53	-0.4	
5	8	83.1	82.4	.55	+0.7	

increases, the incondensible gas volume is compressed, which increases the condenser heat rejection area. As the area and the amount of heat rejection increase, the vapor pressure decreases in a self-regulatory manner. Further description of the variable conductance heat pipe is beyond the scope of this effort.

There are several potential sources of the incondensible gas slug: (1) hydrogen could have been generated due to incomplete passivation of the stainless steel; (2) helium, which was used in the filling fluid transfer operations, could have been absorbed in the working fluid; or (3) trace amounts of atmospheric gases other than oxygen might have remained after preboiling the working fluid. The volume of the incondensible gas was small, however, since the agreement between the internal thermocouple temperature measurements was good. Thus, we believed that the incondensible contaminant was either helium or residual atmospheric contaminant.

3. MEAN AXIAL AND RADIAL TEMPERATURE GRADIENTS

Figure 26 shows the composite temperature gradients for the radial evaporator, ΔT_{er}, condenser, ΔT_{cr}, and axial, ΔT_{ax}, temperature gradients for the planar heat pipe using 32 grams of water and forced convection cooling. These data are averages, based on the mean evaporator and condenser temperatures, respectively, for all forced convection cooled tests. Data has been extrapolated to zero ΔT for zero input power.

a. Thermal Resistance of Heat Pipe

Based on the data in Figure 24, the axial thermal resistance of the device can be calculated as shown in Table X. Thermal resistance, entirely analogous to electrical resistance, is defined by

$$R_T = \frac{\Delta T}{\dot{Q}} \tag{26}$$

where R_T is the thermal resistance ($\frac{^\circ C}{watt}$ or $\frac{^\circ F}{BTU/hr}$), ΔT is the temperature gradient, and $\dot{Q}$ is the heat transfer rate.

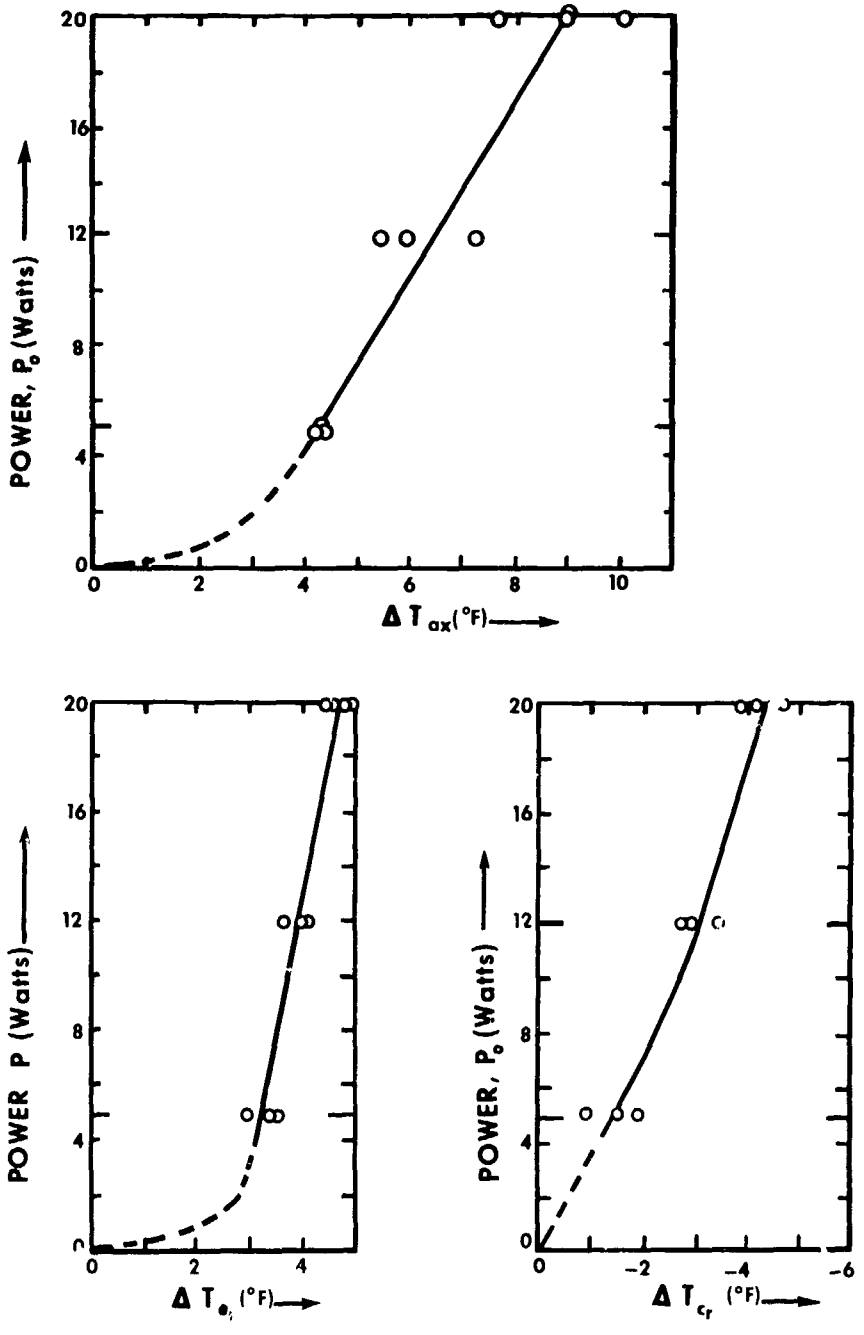

Figure 26. Planar Heat Pipe Equilibrium Temperature Gradients, Forced Convection Cooling and 32 Grams H_2O, 12, and 20 Watts

TABLE X

MEAN THERMAL RESISTANCE CALCULATIONS
FOR PLANAR HEAT PIPE, FORCED CONVECTION COOLED TESTS

Power (w)	Power (BTU/hr)	ΔT_{ax} (°F)	ΔT_{ax} (°C)	$R_{T_{ax}}$ (°C/W)	$R_{T_{ax}}$ (°F/BTU/hr)
5	17.05	3.8	1.83	.367	.194
12	41.9	3.8	2.11	.176	.091
20	68.2	4.6	2.58	.128	.067

Table XI presents a summary of the measured mean external axial temperature gradients (ΔT_{ax}), evaporator radial temperature gradients (ΔT_{er}), and condenser radial temperature gradients (ΔT_{cr}) for both the forced convection and -50°F radiation cocled tests for the planar heat pipe in the near horizontal position with 32 grams of working fluid. Although the internal temperatures range from 53°F to 177°F, the data show remarkable agreement.

b. Film Heat Transfer Coefficient Calculation

The film heat transfer coefficient, h, is defined by the one-dimension convection heat transfer equation given by

$$\frac{Q}{A} = \bar{h}\,\Delta T$$

where ΔT is the difference between the wall and bulk fluid temperature and $\frac{Q}{A}$ in the input heat flux. Since the internal thermocouples rested on the capillary screen and the capillary was saturated, the bulk fluid temperature is that measured by the internal thermocouples. Figure 27 shows the calculated values of the film heat transfer coefficient for an input flux ranging from 61 $\frac{BTU}{hr\ ft^2}$ (5 watts)

TABLE XI

COMPARISON OF AXIAL AND RADIAL TEMPERATURE GRADIENTS,
FORCED CONVECTION AND RADIATION COOLED TESTS
(32 GMS H_2O)

Test Description	ΔT_{ax} (°F)	ΔT_{er} (°F)	ΔT_{cr} (°F)	T_o (°F)	$\bar{T}_i$ (°F)
20w Convection 1 hr	10	4.5	-5.5	71	105.6
20w Convection 1 hr	8.9	4.9	-4.1	79	112.0
20w Radiation .5 hr	10	5.4	-4.9	-50	95.0
20w Radiation 1 hr	9.5	4.8	-5.5	-50	110.6
12w Convection 1 hr	5.9	3.4	-3.5	75	93.6
12w Convection 1 hr	7.2	3.9	-3.3	72	93.1
12w Radiation 1 hr	6.2	1.9	-3.8	-50	50.8
12w Radiation 1.5 hrs.	6.2	2.0	-3.6	-50	50.8
12w Radiation 12.0 hrs.	5.6	4.1	-3.0	+85	177.75
5w Convection 1 hr	4.2	2.9	-1.3	73.5	84.1
5w Convection 1 hr	4.3	2.9	-1.5	76	85.8
5w Radiation 1 hr	7.1	1.1	-4.2	-50	53.7
5w Radiation 2 hrs.	6.4	2.0	-3.6	50	46.6

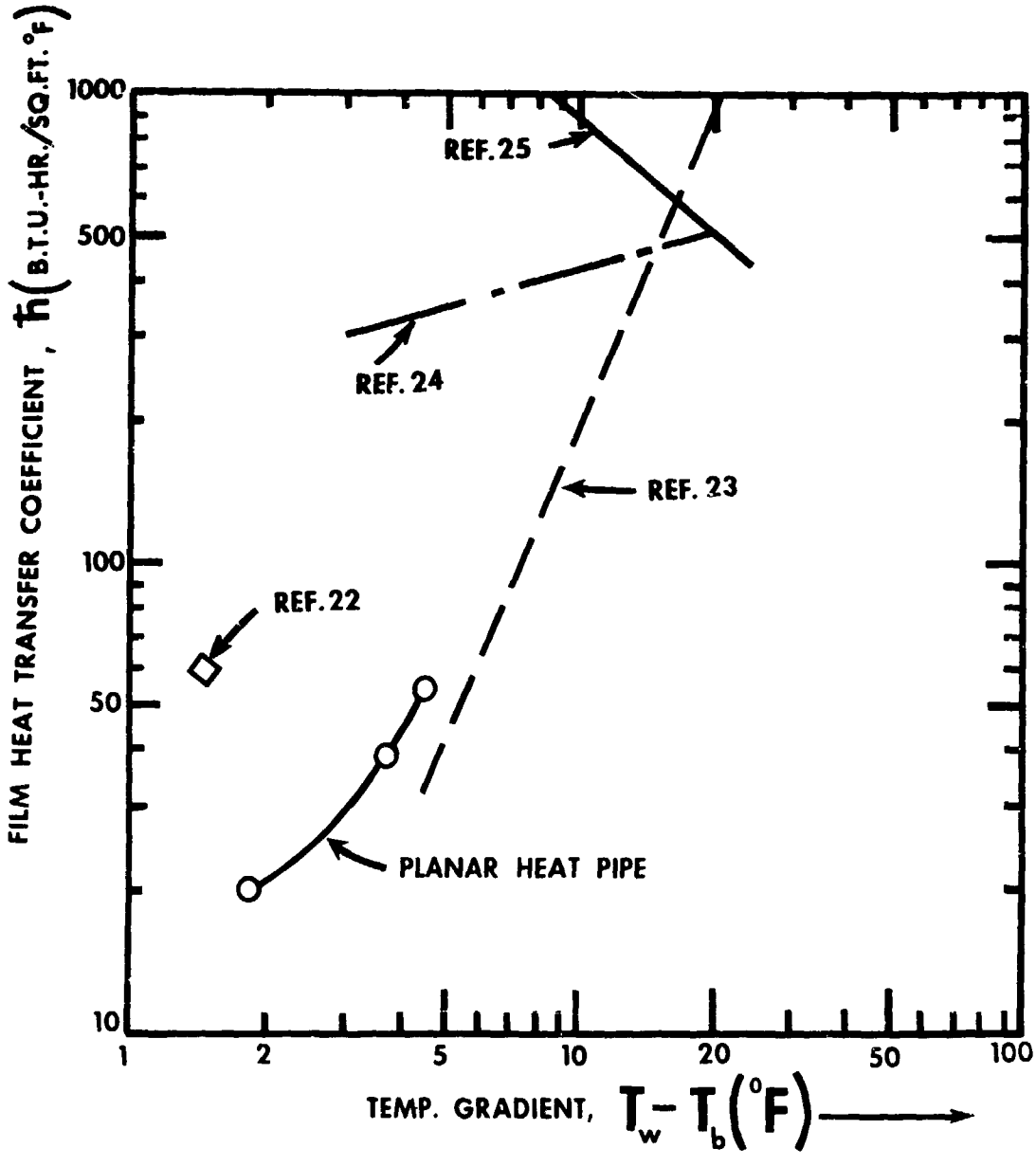

Figure 27. A Comparison of Experimental Convective and Boiling Film Heat Transfer Coefficients

to 246 $\frac{BTU}{hr\ ft^2}$ (20 watts) for the planar heat pipe. The ΔT is based on the measured external and internal evaporator temperatures. The conduction temperature drop through the 0.025-inch stainless steel shell (0.055°F) can be neglected. The heat transfer area is taken as 20 square inches.

The calculated values of the film heat transfer coefficient of the planar heat pipe are based on the 32 gm, near horizontal, forced convection cooling tests. These values compare favorably with the data reported by Jacob (Reference 22) and Kern (Reference 23) for natural convective heat transfer and surface evaporation at atmospheric pressure. The data by Allingham and McClure (Reference 24), and Kunz, et al (Reference 25) were taken for much higher input heat fluxes.

4. ANALYSIS OF CAPILLARY PROPERTIES OF STAINLESS STEEL SCREEN WICK

The capillary wick employed for the planar heat pipe was 100 mesh (100 wires per inch by 100 wires per inch), 60% dense material, with a wire diameter of 0.0045 inch. The thickness of a single layer of screen was measured as .010 inch ±.002 inch. The calculated thickness of two layers of screen, assuming no compression, is then approximately .020 inch.

Kunz, et al, (Reference 26) made porosity measurements of compressed multilayer 100 mesh nickel screen of the same wire size, typically 0.10 inch thick, ranging from 58.5 to 67.9%. The measured wick friction factor was $6.1 \times 10^{+8}$ per sq ft (Reference 18). Calimbas and Hulett measured a wick friction factor of double layer of 120 mesh nickel screen $7.3 \times 10^{+8}$ per sq ft; porosity was not reported (Reference 27).

Wick rise test data of Freggins (Reference 28) and Kunz, et al (Reference 29), for multiple-layer unsintered 120-mesh, and multiple-layer sintered 100-mesh nickel screens show maximum pumping heights of approximately 2 to 4.5 inches. Table XII summarizes the capillary parameters found in the literature for capillary structures similar to that of the planar heat pipe. These data were employed to design the planar heat capillary structure and insure adequate heat transfer capability. For calculation purposes, a wick porosity of 70% was assumed.

TABLE XII

CAPILLARY PROPERTIES OF SCREEN WICKS
(Test Conditions: Water Temperature - 25°C, Pressure-1 Atmosphere)

Wick Configuration	Max. Rise (in)	Friction Factor per ft^2	Porosity, (%)	Reference
Multilayer 120 mesh nickel, clean	2.21	1.539×10^8	-	28
Multilayer 120 mesh nickel, oxidized	3.21	2.67×10^8	-	28
Single layer 120 mesh stainless steel Type 304	-	6.5×10^8	-	27
Double layer 120 mesh stainless steel Type 304	-	8.3×10^7	-	27
Sintered Multilayer 100 mesh nickel	>4.4	6.1×10^8	58.5 - 69.4	29
Sintered Multilayer 200 mesh nickel	12.2	12×10^8	67.8	29
Sintered Multilayer 50 mesh nickel	1.9	1.4×10^8	62.5	29

As described in Section II, the maximum heat input as predicted from the 1.0g wick rise test, given by Equation 25, is

$$Q_{max} = 2\left(\frac{\rho_l h_{vl} \sigma}{\mu_l}\right)\left(\frac{b\delta}{X_T}\right)\left(\frac{g\rho_l}{\sigma}\right)_{wR}\left(\frac{lm}{K_l}\right) \qquad (25)$$

The above equation can be used to calculate the maximum heat transfer capability of the planar heat pipe. Based on the experimental results, the value of lm is at least 1 inch (evaporator elevation) and K_l is approximately 7.0×10^8 sq ft, as measured by Calimbas and Hulett (Reference 27). Assuming these values for maximum rise (lm) and friction factor and fluid parameter values for nominal 120°F operation, the maximum heat transport rate for the planar heat pipe can be computed to be approximately 40 watts, as shown in Appendix III.

The maximum current attainable from the Trygon power supply was 3.0 amps, so that the maximum power that could be applied to the resistance-limited copper plate heaters was approximately 25 watts. Hence, burnout could not be measured for the heat pipe using 32 grams of working fluid.

Equation 25 does not contain an explicit term for working fluid mass; hence, some discussion as to why burnout occurred for small amounts of working fluid is appropriate. Equation 25 assumes the capillary to be initially saturated, hence, the value of lm is maximum. If the capillary is not saturated, i.e., if the amount of working fluid is insufficient, the value taken for lm must be reduced. With the capillary unsaturated, capillary pumping is not maximum and the vapor generation rate may exceed the liquid return flow rate.

Appendix V presents an analysis of the time necessary to deplete the capillary liquid, assuming no capillary return flow. For 16 grams of working fluid, burnout will occur in 1 hour with 5 watts of applied power, and in 12 minutes with 20 watts of applied power assuming no return flow. With 16 grams of working fluid, burnout did not occur after the consecutive 1-hour tests at 5 watts and 12 watts but did occur from the 20 watt, 1-hour test. We concluded that the capillary pumping rate was insufficient to meet the 20-watt vapor generation rate for this amount of working fluid, but was adequate to satisfy the 5-watt and 12-watt vapor generation rates.

5. HEAT PIPE DESIGN REFINEMENT

It would be desirable to reduce the weight and volume of the heat pipe for future tests. The stainless steel shell is the heaviest component, weighing about 0.85 pounds (386 gms). A thinner shell would reduce this weight, as would using aluminum as the shell material, and welding together rather than soldering it.

Some buckling and distortion of the external evaporator face was noted. From ink-blot prints of the evaporator surface, we estimated that only 90% of the surface area was in mechanical contact with the heater surface. For in-vacuum applications, some thermal grease or mechanical bond should be used between the battery case and the heat pipe. We estimate that the weight and volume of the prototype heat pipe could be reduced by at least 50% with no decrease in the heat transport effectiveness.

Some improvement of heat transfer in both the evaporator and the condenser could be realized by employing a sintered screen wick or a porous metal, thus decreasing evaporator and condenser temperature gradients. Use of a sintered wick would increase conductive heat transfer through the wick, which would effectively increase the film heat transfer coefficient and minimize the temperature gradient.

SECTION VI

CONCLUSIONS AND RECOMMENDATIONS

The goals and experimental objectives of this effort were met. The planar heat pipe was designed and fabricated. Operation of the device was stable and repeatable. Comparative testing with the aluminum and copper fins demonstrated the heat pipe's superiority as a heat transfer device. These results lend credibility to the heat-pipe-cooled battery concept. Future experimental efforts will center on testing the planar heat pipe with an actual nickel-cadmium battery.

The radial and axial temperature gradients were measured for applied powers of 5, 12, and 20 watts. The mean axial thermal resistances, based on the external temperature gradient, were 0.194 and 0.067°F/BTU per hr for 5 and 20 watts input power with forced convection cooling of the condenser. Evaporator film heat transfer coefficients, based on the observed radial temperature gradients, were found to be 18.6 and 53.5 BTU/hr/sq ft/°F for input power densities of 61.4 BTU/hr/sq ft. (5 watts) and 245.6 BTU hr/sq ft (20 watts), respectively.

The layered capillary material gave rise to relatively large radial temperature gradients, typically 4 to 5°F, as predicted by natural convection heat transfer theory. Use of sintered or porous metal for the wick would reduce the evaporator and condenser radial temperature gradients.

Passivation of the heat pipe was accomplished by a relatively simple process; there was no evidence of generation of a significant amount of incondensible gas (hydrogen), although a small amount of incondensible gas was present, as noted by a temperature-pressure discrepancy when the device was tested in the vertical position. This gas should be sampled to identify the contaminant.

No attempt was made to minimize the weight and volume of the prototype planar heat pipe. We estimate that the weight and volume could be reduced by at least 50% with no reduction in heat transfer effectiveness. Future devices should be fabricated from thinner stainless steel or aluminum to minimize case weight, and the case should be welded rather than soldered. The capillary material should be permanently bonded to the case shell to eliminate the need for internal springs to anchor the wick to the wall.

APPENDIX I

CALCULATION OF VAPOR INJECTION VELOCITY AND AXIAL PRESSURE LOSS IN RECTANGULAR CHANNEL

The injection and condensation velocity for the planar heat pipe may be determined as described in Section II. The details of the calculation, including supplemental equations, are given below.

Assume that the channel has the same dimensions as the planar heat pipe (3-1/2 x 1/2 x 12 inches), that the working fluid is water, and that the input power is 20 watts. The input power and the vapor generation rate are related by

$$\dot{Q} = \dot{m}_v h_{vl} \tag{27}$$

where h_{vl} is the latent heat of vaporization of the liquid.

The elementary continuity equation is

$$\dot{m}_v = (A \rho_v u_o) \tag{28}$$

where u_o is the vapor injection velocity.

Combining Equations 27 and 28 and solving for u_o, we obtain an expression for the vapor injection velocity in terms of the input power flux, $\dot{Q}/A$, and the vapor properties ρ_v and h_{vl}, given by

$$u_o = \frac{\dot{Q}}{A}\left(\frac{1}{\rho_v h_{vl}}\right) \tag{29}$$

The input power flux is approximately 0.5 watts/in^2, or about 0.1 watt/cm^2. At 122°F, the density of water vapor, ρ_v, and the latent heat of vaporization of water are 0.5×10^{-4} gm/cm^3 and 568.4 cal/gm, respectively. Substituting these values into Equation 29 yields

$$u_o = \frac{(0.1 \text{ watt/cm}^2)\left(0.2388 \frac{\text{cal/sec}}{\text{watt}}\right)}{(0.5 \times 10^{-4} \text{ gm/cm}^3)(568 \times 10^2 \text{ cal/gm})} \simeq 1.0 \text{ cm/sec} \tag{30}$$

The pressure loss in the rectangular channel for a low viscosity vapor is given by Equation 19 (Reference 12).

$$\frac{dp_v}{dx} = -\pi/2(\rho_v u_o^2/a^2)x \qquad (19)$$

where a is the channel halfwidth and x is the channel length. For the planar heat pipe, a is approximately 1.65 inches, or about 4 cm, and x is 6 inches, or approximately 15 cm. Integrating Equation 19 and substituting these values yields

$$\Delta p_v\Big|_{evap} = -\pi/8\rho_v u_o^2 x^2/a^2 = -\pi/8(0.5\times10^{-4}\ gm/cm^3)\frac{225\ cm^2}{16\ sec^2}$$

$$\Delta p_v\Big|_{evap} \simeq 2.5\times10^{-4}\ dyne/cm^2 \simeq 0.5\times10^{-10}\ psi$$

Thus, the vapor pressure loss in the 15 cm evaporator length is approximately 0.5×10^{-10} psi. Due to the geometrical and heat rejection symmetry of the evaporator and condenser, the vapor pressure loss in the condenser is also approximately 0.5×10^{-10} psi. The total viscous pressure drop in the vapor is small ($\sim 1 \times 10^{-10}$ psi) compared to the total vapor pressure of water, which is approximately 1.0 psi for the temperature regime of interest (100°F).

APPENDIX II

CALCULATION OF TEMPERATURE GRADIENT IN CAPILLARY WICK

Two analytical models for heat transfer in the capillary wick are examined quantitatively; each model corresponds to a distinctly different capillary structure and heat transfer mode.

1. THERMAL CONDUCTION MODEL

For a homogenous porous capillary material, heat transfer by thermal conduction through the liquid medium of the composite wick may be described by evaluating the effective thermal conductivity of the composite medium. Corring and Churchill (Reference 14) show the effective thermal conductivity is given by

$$k_T = \frac{k_w}{1+\xi\left(\frac{k_w}{k_1}-1\right)} \tag{31}$$

where ξ is the wick porosity and k_w and k_1 are the thermal conductivities of the liquid and wick material.

The thermal conductivity and the porosity of the stainless steel screen material was 9.4 BTU/hr ft°F (.163 watts/cm°C) and 70%, respectively. The thermal conductivity of water is 0.343 BTU/hr ft°F (0.00369 watts/cm°C). Using these values, the effective thermal conductivity of the wick, from Equation 31, is

$$k_T = \frac{9.4\ \text{BTU/hr ft°F}}{1+(0.7)\left[\frac{9.4}{0.343}-1\right]} = 0.49\ \text{BTU/hr ft°F} = 0.0408\ \text{BTU/hr in°F}$$

The temperature drop through the wick can be computed by employing the one-dimensional thermal conduction equation

$$Q = kA\frac{\Delta T}{\Delta T} \tag{32}$$

Solving for ΔT and evaluating for ΔL 0.020 inches, $k = k_T$ = 0.0408 BTU/hr in. °F, Q = 20 watts, A = 40 in.^{2} (evaporator area), we have

$$\Delta T = \frac{Q}{A}\frac{\Delta L}{k} = 0.5 \text{ w/in.}^2 \left(3.412 \frac{\text{BTU/hr}}{\text{w}}\right) \frac{0.020 \text{ in.}}{0.0408 \text{ BTU/hr in.°F}} = 0.85°\text{F} \quad (33)$$

2. FREE CONVECTION MODEL

For a layered unsintered wick where the screen layers are not in intimate contact with adjacent screen layers, heat transfer can be attributed to natural or free convection in the working fluid, described by

$$Q = hA\Delta T \quad (34)$$

where h is the film, or convective heat transfer coefficient. In general h must be determined experimentally. Assuming h equals 50 BTU/hr ft^2 °F, the temperature gradient through the wick for Q/A = 0.5 watt/in.^{2} can be calculated as

$$\Delta T = \left(\frac{Q}{A}\right)\frac{1}{h} \frac{\frac{0.5 \text{ watts}}{\text{in.}^2}\left(\frac{144 \text{ in.}^2}{\text{ft}^2}\right) 3.414 \frac{\text{BTU/hr}}{\text{watt}}}{50 \text{ BTU/hr ft}^2 \text{ °F}} = 4.8°\text{F} \quad (35)$$

Thus, the conduction heat transfer model predicts a temperature gradient of 0.85°F, and the free convection model predicts a temperature gradient of 4.8°F. Since the actual wick structure was layered rather than homogenous, the free convection model is more appropriate to this investigation. (Experimental measurements described in Section 4 show the evaporator and condenser equilibrium temperature gradients were 4 to 5°F for 20 watts applied power).

For planning future work, note that the evaporator and condenser radial temperature gradients could be reduced by employing a sintered, bonded wick to increase the thermal conduction heat transfer.

APPENDIX III

CALCULATED MAXIMUM HEAT TRANSFER RATE OF PLANAR HEAT PIPE

Using Equation 25, the maximum heat transfer rate of the planar heat pipe is

$$\dot{Q}_{max} = 2 \left(\frac{\rho_l h_{vl} \alpha}{\mu_l}\right)\left(\frac{b\delta}{X_T}\right)\left(\frac{g\rho_l}{\sigma}\right)_{WR} \frac{lm}{K_l} \qquad (25)$$

The first and third terms may be numerically evaluated from physical data handbooks. Assume at a temperature of 50°C (122°F), then the values for the liquid parameters in the above equation are as follows:

$$\rho_l = 0.989 \text{ gm/cm}^3$$

$$h_{vl} = 568.4 \text{ cal/gm at } 50°C$$

$$\sigma = 67.91 \text{ dynes/cm}^2 \text{ at } 50°C$$

$$\mu_l = 0.5494 \text{ poise at } 50°C$$

$$\rho_{l_{WR}} = 1.0 \text{ gm/cm}^3 \text{ at } 25°C$$

$$\sigma_{WR} = 72 \text{ dynes/cm}^2 \text{ at } 25°C$$

From the geometry of the heat pipe and wick

$$b = 3.5 \text{ inches}$$

$$\delta = 0.020 \text{ inch}$$

$$X_T = 12 \text{ inches}$$

so that

$$\frac{b\delta}{X_T} = 0.015 \text{ cm}$$

Assume the maximum rise, lm, to be one inch and the value of the wick friction factor $K_1 = 7 \times 10^8$ per sq ft, or 7.35×10^5 per sq cm. These

selected values of lm and K_1 are validated by data listed in Table XII. Then the estimated value of $\frac{lm}{K_1}$ is

$$\frac{lm}{K_1} = \frac{2.54 \text{ cm}}{7.53 \times 10^5 \text{ sq cm}} = 0.337 \times 10^{-5} \text{ cm}^3$$

Substituting these values for all four terms in Equation 25 yields

$$Q_{max} = 2 \left[\frac{0.989 \frac{gm}{cm^3} \times 568.4 \frac{cal}{gm} \times 67.91 \frac{gm\ cm}{cm^2\ sec^2}}{0.5494 \frac{gm}{cm} \text{ cm}} \right] \left[0.15 \text{ cm} \right]$$

$$\left[\frac{980 \frac{cm}{sec^2} \times \frac{1 \text{ gm}}{cm^3}}{72 \frac{gm\ cm}{cm^2} sec^2} \right] \left[0.337 \times 10^{-5} \text{ cm}^3 \right]$$

The maximum heat transport rate for the prototype planar heat pipe is, thus

$$Q_{max} = 40.2 \text{ watts}$$

APPENDIX IV

CALCULATIONS OF THE AMOUNT OF WATER NECESSARY TO SATURATE CAPILLARY WICK

Assume the wick thickness is .020 inch with a porosity (ratio of void volume to total volume) of 70%. The volume, V, of the wick is approximately

$$V = \text{thickness} \times \text{area} = (0.02)(3\text{-}1/2 \times 12 \times 2 + 1/2 \times 12 \times 2)\ \text{in.}^3$$

$$V = (0.02)(96) = 1.92\ \text{in.}^3$$

The void volume, V', of the wick is simply

$$V' = \xi V = (0.7)(1.92) = 1.344\ \text{in.}^3$$

The amount of liquid necessary to saturate this volume is

$$m = V'\rho_l \tag{36}$$

Evaluating Equation 36 numerically yields

$$m_{H_2O} = (1.152\ \text{in.}^3)\left(1\ \frac{\text{gm}}{\text{cm}^3}\right)\ 16.39\ \frac{\text{cm}^3}{\text{in}^2} = 22.03\ \text{gm}$$

Thus, it requires approximately 22 gms of water to saturate the wick. This calculation assumes an ideal wick configuration, with no separation or undulations between the screen layers.

APPENDIX V

VAPORIZATION RATE CALCULATIONS FOR NONEQUILIBRIUM OPERATION

Calculate the amount of time necessary to evaporate all the fluid in the planar heat pipe with 16 grams of fluid at applied powers of 5 and 20 watts.

For 5 watts, assume the heat of vaporization of water is 578 $\frac{cal}{gm}$, which corresponds to approximately 90°F operation. For 20 watts, assume the heat of vaporization is 568.4 $\frac{cal}{gm}$, which corresponds to operation at approximately 122°F.

Assume initially that half (8 grams) of the water is in the evaporator and that the liquid is not replenished by the capillary pump. The total amount of heat necessary to vaporize 8 grams of water at 90°F and 122°F, respectively, is

At 5 watts

$$Q_{T_5} = (8\ gm)\ 578\ \frac{cal}{gm} = 4630\ cal$$

At 20 watts

$$Q_{T_{20}} = (8\ gm)\ (568.4\ \frac{cal}{gm}) = 4550\ cal$$

The times for t_{5w} and t_{20w} complete evaporation at 5 watts (119 $\frac{cal}{sec}$) and 20 watts (4.76 cal/sec), respectively, are

$$t_{5w} = \frac{Q_{T_5}}{\dot{Q}_5} = \frac{4630\ cal}{1.19\ \frac{cal}{sec}} = 3900\ sec = 1.08\ hours$$

$$t_{20w} = \frac{Q_{T_{20}}}{\dot{Q}_{20}} = \frac{4550\ cal}{4.76\ \frac{cal}{sec}} = 957\ sec = 0.21\ hour \simeq 12\ minutes$$

Thus, burnout would occur after 12 minutes when 20 watts was applied if the capillary pump did not replenish the evaporator.

REFERENCES

1. E. W. Brooman and J. McCallum, Heat Transfer in Sealed Nickel Cadmium Spacecraft Cells and Batteries, Battelle Memorial Institute, Technical Report, AFAPL TR 69-21, prepared under Contract Nr. AF33(615)-3701, 30 April 1969.

2. S. Gross, "Heat Generation in Sealed Batteries," Energy Conversion Journal, 9, 55, 1969.

3. Private Communication with Dr. J. Lander, Air Force Aero Propulsion Laboratory, Wright-Patterson AFB, Ohio, February 1970.

4. G. M. Grover, T. P. Cotter, and G. F. Erickson, "Structures of Very High Thermal Conductance," J. Appl. Phys., 35, 1990, 1964.

5. E. Hausmann and E. P. Slack, Physics, D. Van Nostrand and Co., Inc., Princeton, New Jersey, 4th ed., p180, 1957.

6. A. W. Adamson, Physical Chemistry of Surfaces, Interscience Publishing Co., Inc., New York, 2nd ed., p 317, 1967.

7. L. M. Milne-Thompson, Theoretical Hydrodynamics, The Macmillan Company, New York, 5th ed., p446, 1968.

8. H. R. Kunz, L. S. Langston, B. H. Hilton, S.S. Wyde, and G. H. Nashick, Vapor-Chamber Fin Studies, Transport Properties and Boiling Characteristics of Wicks, Pratt and Whitney Aircraft, NASA Contractor Report, NASA-CR-812, prepared under Contract Nr. NAS-3-7622, p7, June 1967.

9. A. E. Scheidegger, The Physics of Flow Through Porous Media, (The Macmillan Company, New York, Revised Edition, p37ff, 1960.

10. Ibid, p87.

11. Kunz, et al, op cite, p105.

12. B. K. Knight, Jr., and B. B. McInteer, Laminar Incompressible Flow in a Channel with Porous Walls, Report LADC 5309, Los Alamos Scientific Laboratory of the University of California, undated.

13. W. H. McAdams, Heat Transmission, McGraw Hill Book Co., Inc., New York, 3rd ed., p370, 1954.

14. R. L. Gorring and S. W. Churchill, "Thermal Conductivity of Heterogeous Materials," Chem. Engr. Prog., 57, No. 7, p53ff, July 1961.

15. McAdams, op cite, p373.

16. D. Q. Kern, Process Heat Transfer, McGraw Hill Book Co., Inc., New York, p377, 1950.

REFERENCES (Contd)

17. Kunz, et al, op cite, pp13-26.

18. Private Communication with Dr. J. Lander, Air Force Aero Propulsion Laboratory, January 1970; this passivation process has been employed by battery manufacturers in preparing stainless steel cases for sealed spacecraft cells. Heat pipe fabricators have employed much more sophisticated processes for stainless steel water heat pipe with varying degrees of success and repeatability.

19. The Electrical Research Association, 1967 Steam Tables, St. Martins Press, New York, pp2-3, 1967.

20. L. R. Kelley, Estimated Weight Penalties Incurred by Inboard Placement of a Two Kilowatt Nickel Cadmium Battery, TRW Systems Group, Report Nr. 68-8526.16h-06, 1969.

21. McAdams, op cite, p175.

22. McAdams, op cite, p373.

23. Kern, op cite, p474.

24. W. D. Allingham and J. A. McEntire, "Determination of Boiling Film Coefficient for a Heated Horizontal Tube in Water-Saturated Wick Material," J. Heat Transfer, February 1961, pp74-76.

25. Kunz, et al, op cite, p148.

26. Ibid, p38, p105.

27. A. T. Calimbas and R. H. Hulett, "Avionics Application of a Heat Pipe," 4th Intersociety Energy Conversion Engineering Conference, Washington, D. C., p1017, September 22-26, 1969.

28. R. A. Freggens, "Experimental Determination of Wick Properties for Heat Pipe Applications," 4th Intersociety Energy Conversion Engineering Conference, Washington, D. C., p888ff, September 22-26, 1969.

29. Kunz, et al, op cite p121.